의학박사 학위논문

Development and clinical usefulness evaluation of mesh-type 3D modeling technique for 3D tumor localization

종양의 3차원적 위치 파악을 위한 메쉬 구조의 3D 모델링 기술 개발 및 임상적 유용성 평가

2022년 2월

서울대학교 대학원
의학과 의공학 전공

석 준 걸

Ph.D. Dissertation of Medicine

Development and clinical usefulness evaluation of mesh-type 3D modeling technique for 3D tumor localization

종양의 3차원적 위치 파악을 위한 메쉬 구조의 3D 모델링 기술 개발 및 임상적 유용성 평가

February 2022

Department of Biomedical Engineering
The Graduate School
Seoul National University

Jungirl Seok

Development and clinical usefulness evaluation of mesh-type 3D modeling technique for 3D tumor localization

지도교수 김 희 찬

이 논문을 의학박사 학위논문으로 제출함
2021년 10월

서울대학교 대학원
의학과 의공학 전공
석 준 걸

석준걸의 박사 학위논문을 인준함
2022년 1월

위 원 장	최 진 욱	(인)
부위원장	김 희 찬	(인)
위 원	권 택 균	(인)
위 원	정 은 재	(인)
위 원	진 영 주	(인)

Development and clinical usefulness evaluation of mesh-type 3D modeling technique for 3D tumor localization

By

Jungirl Seok

(Directed by Hee Chan Kim, PhD)

A thesis submitted to the Department of Medicine in partial fulfillment of the requirements for the Degree of Doctor of Philosophy in Biomedical Engineering at Seoul National University College of Medicine

January 2022

Approved by Thesis Committee:

Chair	Jin Wook Choi	(Seal)
Vice Chair	Hee Chan Kim	(Seal)
Examiner	Tack-Kyun Kwon	(Seal)
Examiner	Eun-Jae Chung	(Seal)
Examiner	Young Ju Jin	(Seal)

Abstract

Development and clinical usefulness evaluation of mesh-type 3D modeling technique for 3D tumor localization

Jungirl Seok

Department of Biomedical Engineering
The Graduate School
Seoul National University

Background: As a method of three-dimensional (3D) localization of tumor, 3D printing is introduced to medicine. However, the high costs and lengthy production times required have limited their application.

Objectives: The goal of the first study was to develop a new and less costly 3D modeling method, “mesh-type 3D modeling”, to depict organ–tumor relations. The second study was designed to evaluate the clinical usefulness of a personalized mesh-type 3D-printed thyroid gland model for obtaining informed consent.

Methods: For the mesh-type 3D modeling, coordinates were extracted at a specified distance interval from tomographic images, connecting them to create mesh-work replicas. Adjacent constructs were depicted by density variations, showing anatomical targets (i.e., tumors) in contrasting colors. A randomized, controlled prospective clinical trial (KCT0005069) was designed. A total of 53 patients undergoing thyroid surgery were randomly assigned to two groups: with or without a 3D-printed model of their thyroid lesion upon obtaining informed consent. A U-Net-based deep learning architecture and the mesh-type 3D modeling technique were used to fabricate

the personalized 3D model.

Results: To establish the mesh-type 3D modeling technique, an array of organ-solid tumor models was printed via a Fused Deposition Modeling 3D printer at a lower cost ($0.05 USD/$cm^3$) and time expenditure (1.73 min/cm^3). Printed models helped promote visual appreciation of organ-tumor anatomy and adjacent tissues. In the prospective clinical study, the mean 3D printing time was 258.9 min, and the mean price for production was USD 4.23 for each patient. The size, location, and anatomical relationship of the tumor with respect to the thyroid gland could be effectively presented. The group provided with personalized 3D-printed models significantly improved across all four categories (i.e., general knowledge, benefits of surgery, risks of surgery, and satisfaction; all $p < .05$). All patients received a personalized 3D model after surgery and found it helpful toward understanding the disease, operation, and possible complications, as well as enhancing their overall satisfaction.

Conclusion: The personalized 3D-printed thyroid gland model may be an effective tool for improving a patient's understanding and satisfaction during the informed consent process. Furthermore, the mesh-type 3D modeling reproduced glandular size/contour and tumor location, readily approximating the surgical specimen. This newly devised mesh-type 3D printing method may facilitate anatomical modeling for personalized care and improve patient awareness during informed surgical consent.

Keywords: mesh-type 3D modeling; 3D printing; informed consent; thyroid gland; fused deposition modeling; deep learning

Student Number: 2014-21979

Table of Contents

List of Tables

List of Figures

List of Abbreviations

- CT: Computed Tomography
- DICOM: Digital Imaging and Communications in Medicine
- FDM: Fused Deposition Modeling
- GUI: Graphic User Interface
- MRI: Magnetic Resonance Imaging
- PACS: Picture Archiving and Communication System
- SD: Standard Deviation
- SLA: Stereolithography
- STL: Stereolithography

Chapter 1. Introduction

1.1. Study Background

Tumor localization helps identify surrounding landmarks, accurately remove the lesion, and anticipate possible complications. Accurate localization is essential in laparoscopic surgery where the specimen cannot be directly touched by the surgeon [1]. In thyroid cancer, a head and neck cancer typically requiring surgery, a previously dissected neck may pose a significant surgical challenge requiring intraoperative localization of small lymph node metastasis [2]. Even in radiotherapy, accurate localization of a lesion reduces unnecessary dose and minimizes complication risk [3].

As regards lesion localization using radiologic image data, a previous study proposed that three-dimensional (3D) visualization is beneficial for surgical planning and diagnosis as compared to 2D images, because it affords better information on the shape of structures [4]. Recently, a method for 3D segmentation of lesions using tomographic image data and deep learning has also been proposed [5]. Further studies have suggested visualizing 3D images using augmented reality [6,7]. One of these studies demonstrated promising results indicating that augmented reality may potentially be utilized as a tool for visualizing head and neck cancer imaging and pre-surgical localization of target structures [6].

Three-dimensional printing is another proposed method to visualize 3D images. The 3D-printed anatomical models are widely used in surgical fields, particularly in orthopedic and maxillofacial specialties, as operative guides or templates for surgical planning, implant design, molding of prosthetics, and patient selection [8]. Recently, 3D-printed phantom models have been studied [8-12], for patient education in particular [9,10], and also for evaluating disease states and expediting pre-operative preparations [12].

The time when such patient education is most needed may be the stage of obtaining informed consent. The term “informed consent” first appeared in a 1957 precedent (Salgo vs. Leland, Stanford Junior University Board of Trustees), when the courts helped to establish the role of informed consent in modern medical practice [13]. This legislation requires that a patient be provided information on the benefits and risks of a medical procedure by an experienced physician before it is performed, which allows patients to actively participate in making decisions and protects physicians from litigation [14]. However, several studies have shown that patients lack recall

and possess insufficient knowledge for granting consent [14-18]. Accordingly, additional time is needed to explain all the details, and an insufficient explanation arising from the time-consuming informed consent process could cause a dispute and interrupt the mutual rapport between physician and patient [19].

In order to enhance a patient's understanding, supplementary tools for informed consent have been introduced. A systematic review of the multimedia consent program of the 2000s and early 2010s (e.g., animation, video, or Microsoft PowerPoint) showed that the use of multimedia as auxiliary tools improved a patient's comprehension [20]. Likewise, there are reports that visual aids used to supplement verbal descriptions allow better conceptualization and processing of the information delivered [21,22]. Among visual-aid tools, 3D models may depict the visual aspects of procedures more effectively. However, such models have not yet proved cost-effectiveness, with the expense and time invested acknowledged as shortcomings [8-10]. The cost of producing the 3D-printed model ranges from hundreds to thousands of dollars depending on the type of printing material used [23]. Regarding the modeling and printing time, in a study on a 3D-printed replica model of the pulmonary artery, the design and printing processes required 8 h and 97 h, respectively [24]. For these reasons, although many studies have been performed on methodologies for patient-specific (i.e., personalized) modeling according to various anatomical sites or different purposes such as surgical guidance or medical training [25-29], their usefulness in a clinical setting has only been demonstrated in a few studies [8,9,30,31].

1.2. Purpose of Research

A mesh-type 3D modeling technique was devised to solve the major disadvantages of 3D printing: time and cost. Since the technique is a modeling method, it is applicable to any 3D printing type, such as fused deposition modeling (FDM) or stereolithography (SLA), and any printing material. Owing to its affordable hardware and lower materials cost, the FDM was chosen in this research. However, this printing type has disadvantages such as low print quality and slow speed. Therefore, as part of this study, an experiment was conducted to preliminarily investigate the efficacy of the mesh-type 3D modeling technique for solid tumors in reducing the cost and printing time without loss of organ-tumor anatomical relationships.

Furthermore, to demonstrate the clinical use of mesh-type 3D printing, a

randomized prospective study on obtaining informed consent was conducted using personalized 3D-printed models of patients' thyroid glands and tumors. The thyroid gland is a soft-tissue organ in which lesions exist, sometimes at the border, and this positional relationship is an important consideration for the extent of the surgery. Therefore, the thyroid gland was considered as a suitable organ to reveal the advantages of the mesh-type 3D modeling technique.

For the study, the deep learning technique was adapted for personalized thyroid segmentation because the size and shape of each patient's thyroid gland was different, making it essential to detect the area of the thyroid gland using artificial intelligence to reduce the time and labor for segmentation. Relevant previous studies on deep learning and artificial intelligence have mostly focused on increasing outcome indicators, such as accuracy but have not examined their use and utility. Therefore, another research topic was to develop an application utilizing a trained deep learning model and supplementing the inference, since it was hypothesized that the deep learning model would not perfectly achieve 100% accuracy for thyroid gland segmentation.

This doctoral research aims to achieve 3D lesion localization and devise a model for obtaining informed consent. This effort will potentially serve as a cornerstone for surgical guidance or presurgical models, manufacturable swiftly and inexpensively.

Chapter 2. Materials and Methods

2.1. Mesh-Type 3D Reconstruction

2.1.1. Concept of Mesh-Type 3D Reconstruction

Mesh-type 3D reconstruction is a newly devised method in which a tumor is expressed as a closed 3D structure (e.g., sphere), and the normal tissue that surrounds or partially overlaps the tumor is configured in a mesh form (**Figure 1**). In addition, when anatomical division between normal tissues is necessary (e.g., upper and middle lobes of the right lung), it is possible to visually distinguish them by adjusting the density of the mesh (**Figure 2**).

Using this method, the normal tissue and lesion could even be distinguished in a 3D printer that prints in a single color. In addition, since the mesh structure is hollow, it was expected that cost reduction would be possible by reducing the amount of material required for 3D printing.

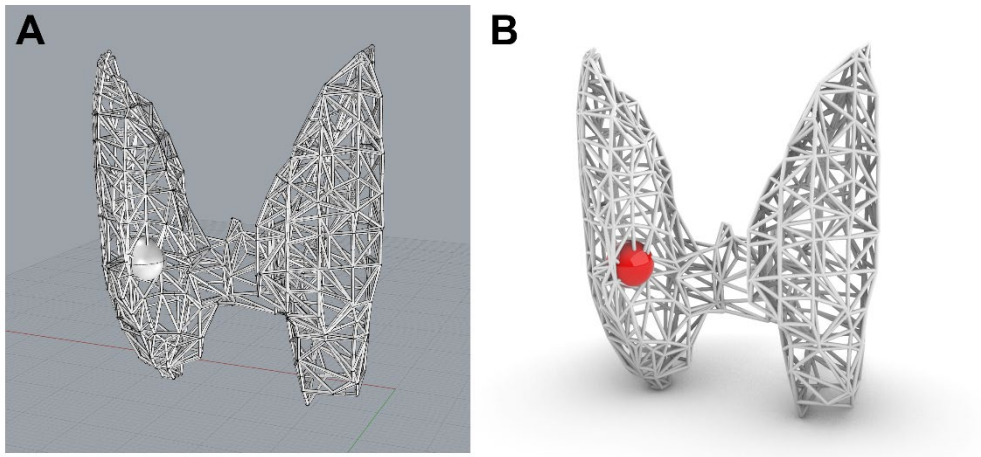

Figure 1. Exemplary image of the thyroid cancer model (A) and rendered image of the mesh in white and tumor in red (B). The lesion is expressed as a sphere, and the thyroid parenchyma is represented by a mesh structure.

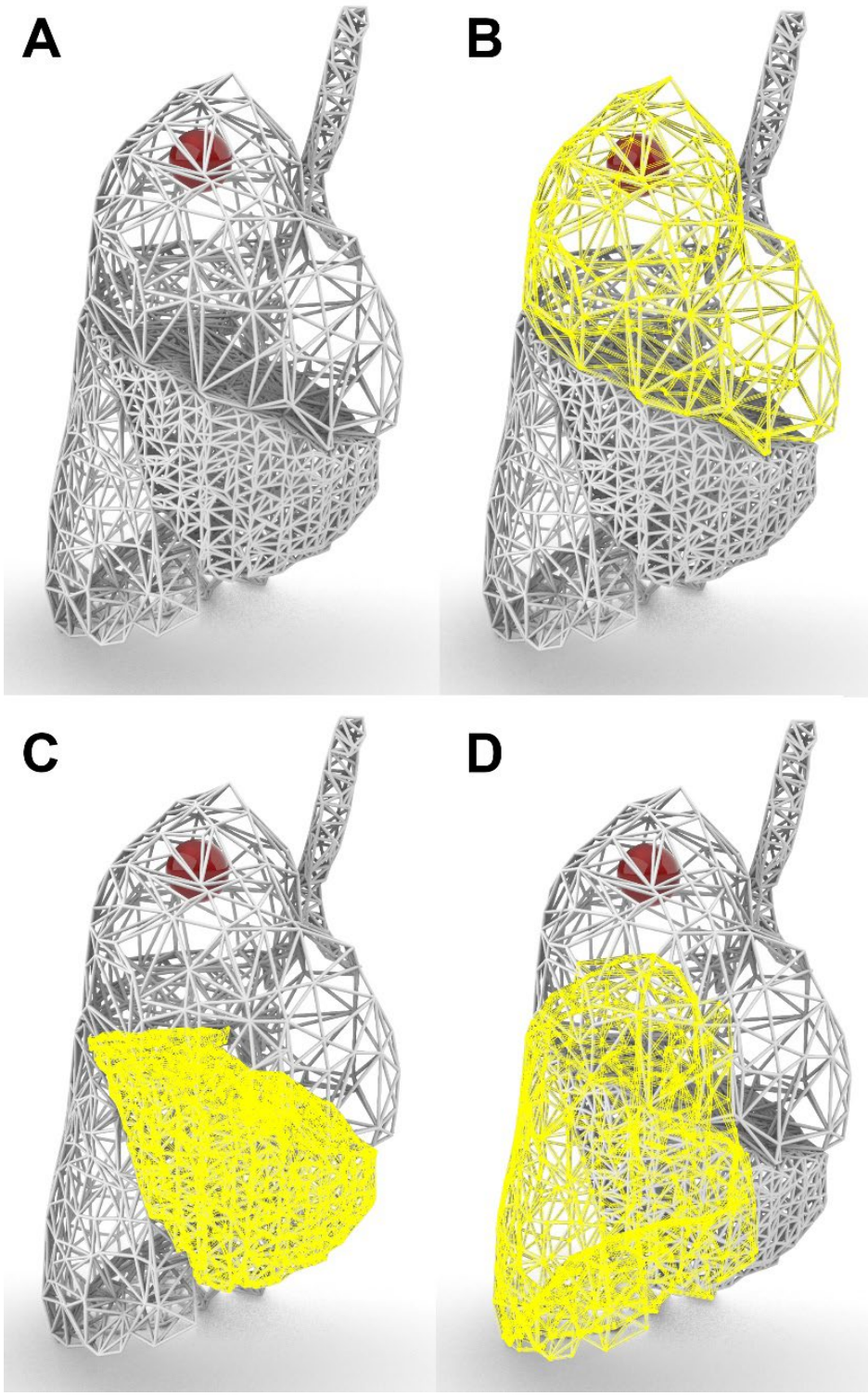

Figure 2. Rendered images of lung cancer model (A). The upper, middle, and lower lobes are highlighted in yellow (B, C, and D, respectively). Each lobe can be distinguished from each other by their different mesh densities.

2.1.2. Mesh-Type 3D Modeling Process

In the modeling process, it is necessary to segment normal structures and lesions that require 3D-printing from Digital Imaging and Communications in Medicine (DICOM) files, which are acquired using computed tomography (CT) or magnetic resonance imaging (MRI) and stored in a hospital system. For this process, only image information needs to be extracted from the DICOM file. The image file could be exported in an image format such as JPEG or PNG file from the picture archiving and communication system (PACS) or extracted from the DICOM file using Python's *pydicom* library [32].

In this experiment, the specific segmentation and labeling, termed "annotation" was performed using the *Labelme* application (https://github.com/wkentaro/labelme, accessed on 28 September 2021). The annotation for each slice was exported to a JSON file (**Figure 3**).

The segmented information with the same label was stacked as a 3D array, and the size of this array represented the number of images, the height of the image, and the width of the image, respectively. Then, the array was reconstructed to reflect the actual size using "pixel spacing" and "slice thickness" value stored in the DICOM file. The reconstructed voxel was 1 mm in size; the ratio of the actual size of the organ can be adjusted at this point. For example, if the ratio was 1:1 (i.e., 1.0), the size (volume) of the array reflected the actual size (volume) of the organ, and if it was 2:1 (i.e., 0.5), the size of each of the 3D axes of the array was halved, and thus the volume was reduced by 1/8th. Afterward, the 3D array was converted into a closed 3D object using the Python *trimesh* library (https://github.com/mikedh/trimesh, v2.38.24, accessed on 8 December 2019), and then the surface was smoothed using the Laplacian smoothing technique (**Figure 4**) [33].

A 3D object created using the *trimesh* library has a surface composed of a triangular plane (facet) connecting three points (vertex). Using this information, instead of a triangular plane, each vertex is expressed as a sphere, and a line connecting the two vertices constituting a facet is expressed as a column to compose a mesh structure (**Figure 5**).

The process of transforming each coordinate into the mesh structure was implemented in *rhino.python*, which is an embedded library within the commercially available 3D modeling software Rhinoceros 3D (version 6.0; Robert McNeel & Associates, Washington DC, USA).

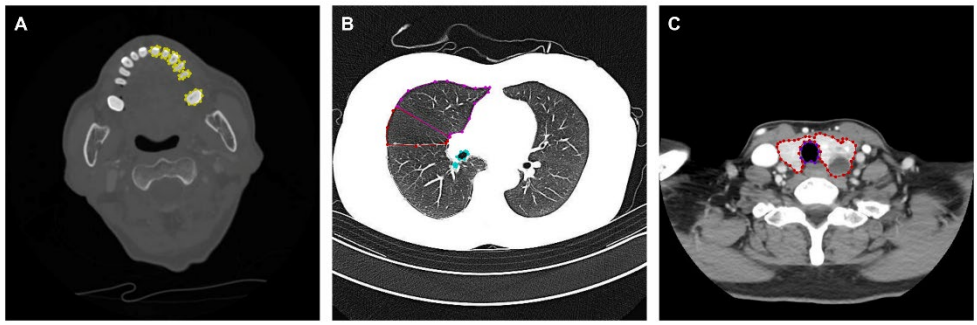

Figure 3. Annotation using *Labelme* application: tooth (A), lung and trachea (B), and thyroid gland (C).

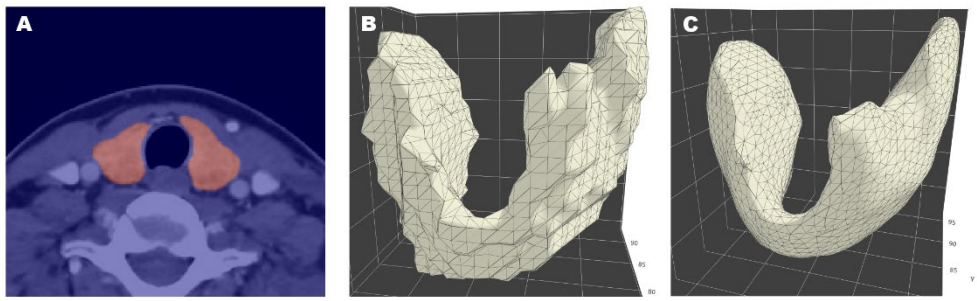

Figure 4. Prototype of mesh-type 3D modeling: segmentation of thyroid gland in tomographic image (A); reconstruction via triangular mesh (B); and surface smoothing (C). This figure has been reproduced with permission from the publisher.

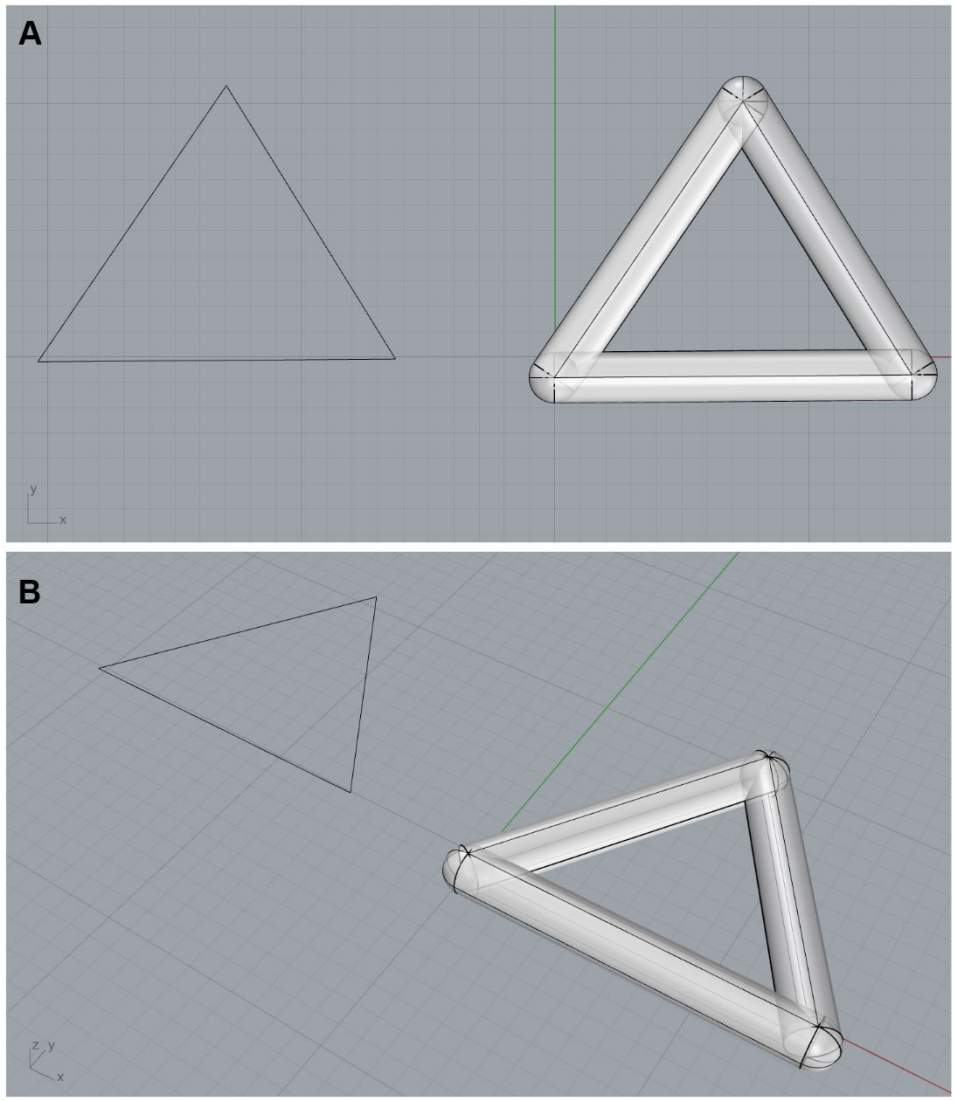

Figure 5. Exemplary image of mesh-structure transformation of a plane composed of three points (top view, A; perspective view, B): three points are expressed as a sphere, and a line connecting two points is expressed as a column.

2.1.3. 3D Printer and Slice Software

A two-color 3D printer (3DWOX 2X; Sindoh, Seoul, Korea) and its slicer software (3DWOX Desktop; Sindoh, Seoul, Korea) were used throughout all 3D printing processes, and the default slicer parameters were unchanged (**Table 1**). The printer is classified as an FDM printer, which uses polylactic acid (PLA) as the printing material. The dual extruder of the printer allows two colors to be used.

2.1.4. Mesh-Type 3D Printing Experiment

For a total of 6 patients who underwent surgery for tumors in different locations (thyroid, nasal cavity, breast, and lung), anatomical models were produced. The size of the printed material, ratio of the size to the actual organ, printing time①, post-processing time②, and cost were calculated. Only the material cost was calculated, excluding labor costs for 3D modeling, printing, and supporting material removal. It was impossible to calculate the labor costs because the time and skill required for those processes were trivial.

The Institutional Review Board (IRB) at the National Cancer Center, Korea, approved the study protocol (No. NCC2020–0248). No patient data was collected, so required informed consent was waived.

① Printing time, which included the time taken for a technician to download a stereolithography (STL) file, transfer the file to the 3D printer, and print the model.
② Post-processing time was measured as the time needed to remove the support material, which the slicer program applied automatically.

Table 1. Manufacturer's default parameters of the slicer software.

Basic Setting	
Layer Height	0.20
Infill Density	15%
PLA Diameter	1.75 mm
Nozzle Temperature	200°
Build Plate Temperature	60°
Shell Wall Thickness	0.8 mm
Support	
Support Pattern	Zigzag
Support Density	20%
Support Overhang Angle	60°
Support Horizontal Expansion	0.8 mm
Support Z-Distance	0.2 mm
Build Plate Adhesion	
Build Plate Adhesion	
Type	Raft
Raft Top-Layers	2 mm
Raft Linewidth	1 mm
Base Quality	
Linewidth	0.3 mm
Wall Linewidth	1.0 mm
Raft Printing Speed	20 mm/s
Speed	
Printing Speed	40 mm/s
Travel Speed	130 mm/s
Initial Layer Speed	20 mm/s
Infill	
Infill Type	Auto
Infill Pattern	Lines Pattern
Retraction	
Retraction Speed	30 mm/s
Retraction Distance	6 mm/s
Retraction Minimum Travel	1.50 mm
Cleaning Tower	Used when the tumor size is large

2.2. Deep Learning for Thyroid Gland Detection

2.2.1. Deep Learning Model Architecture

The thyroid gland is a soft-tissue organ, so it may not show a constant enhancement in CT. Furthermore, the size and characteristics of the thyroid gland and thyroid lesions are different for each individual, making the deep learning technique an optimal methodology for detecting an individual's thyroid gland.

To develop a deep learning model for thyroid gland segmentation, an architecture based on U-Net [34], one of the most widely used models for medical image detection, was designed (**Figure 6**). The deep learning model was not intended to detect the thyroid nodule, as not every thyroid lesion possessed clinical significance for decision making.

2.2.2. Dataset Preparation

A study protocol for the deep learning modeling was reviewed and approved by the IRB of the same institute (No. NCC2019-0206), which granted a waiver of informed consent because the CT series was stored without containing any personal information.

To train the deep learning model, 106 CT series obtained for patients who underwent thyroidectomy surgery from January to June 2013 were used. Each CT series was taken with contrast media according to the "Thyroid CT" protocol of the institute. Each series consisted of about 120 slices obtained from the skull base to the thoracic inlet. The images were converted from a DICOM into JPEG file. The slice thickness was fixed at 2.5 mm, and the pixel spacing was about 0.45 mm per pixel.

The size of the original image was 512 × 512 pixels, with a resolution of 96 dots per inch and depth of 24 bits. All images were cropped at a size of 256 × 256 pixels because the thyroid gland entered the area of 256 × 256 pixels in the center of the image.

Since the image is in grayscale, the size of the color channel was only one. Therefore, the input data for the deep learning model has the form of a 3D array, and the size is 256, 256, and 1 for each dimension, representing height, width, and number of color channels, respectively.

The annotation of the thyroid gland for the training of the deep learning model was performed by using the *Labelme* application. Another experienced thyroid surgeon (CHR) reviewed and verified the initial labeling.

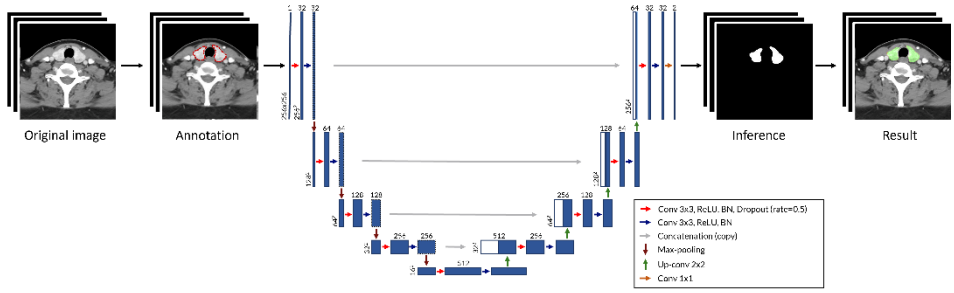

Figure 6. Deep learning model architecture for thyroid gland detection based on U-Net. At each step, the blue box represents a multichannel (feature) layer, and each white box represents a concatenated layer. The number at the top and bottom-left of each box indicates the number of channels and 2D size of the layer, respectively (Conv, convolution layer; BN, batch normalization).

2.2.3. Training, Data Augmentation, and Loss Function

The 106 CT series collected for the deep learning model training were randomly divided into three sets at a ratio of 3:1:1 for each training, validation, and test, resulting in numerical values of 63, 21, and 23, respectively.

For the loss function for thyroid gland segmentation, the Dice coefficient was used, which is defined as follows:

$$Dice\ (y, y') = \frac{2\ |\ y\ \cap y'\ |}{|\ y\ |\ \cup\ |\ y'\ |}$$

where y represents the ground truth and y' is the inference. Accordingly, the loss function was defined as follows:

$$L^{DICE} = 1 - Dice\ (y, y') = 1 - \frac{2\ |\ y\ \cap y'\ |}{|\ y\ |\ \cup\ |\ y'\ |}$$

During the training, early stoppage was implemented; therefore, the training was instructed to stop when L^{DICE} was not improved over 200 epochs. The image augmentation method was adjusted at every training epoch using the *imgaug* library (https://github.com/aleju/imgaug, accessed on 01 February 2020). Each image was transformed by the following methods, with a 70% random probability: (1) size scaling from -30% to +30% for each width and height; (2) rotation from -10° to +10°; (3) shearing from -10° to +10°; (4) input coarse noise signal (coarse dropout) with a probability of 5–10% per pixel over the entire 10–20% of the image area. Finally, the image was horizontally flipped with a 50% probability.

The batch size was set to 16, and the training was performed using Titan V (NVIDIA Co., Santa Clara, CA, USA) as a graphic processing unit in a personal computer.

2.3. Production of 3D Thyroid Gland Reconstruction Application to Deploy Deep learning Model

2.3.1. Concept of the Application

It is technically difficult for deep learning to achieve 100% accuracy. Therefore, a graphic user interface (GUI)-based application that deploys the deep learning model was developed to correct the area that is incorrectly inferred by the deep learning model. In addition, the application enabled

clinicians to mark thyroid nodules on CT images, since there is no reason for all nodules to be three-dimensionally reconstructed. In the application, nodules that could affect surgical extent are indicated by marking lesions manually. The application was developed and named STIR 3D (Stacked Thyroid Images Reconstruction to 3D model; **Figure 7**).

2.3.2. Functions of the Application

The application proceeds in the following order: (1) load images, (2) load DICOM preferences (slice thickness and pixel spacing), (3) inference of deep learning model, (4) add (draw)/remove (erase) mask, (5) add/remove thyroid nodule, and (5) export to files.

When the inference of the deep learning model is finished, the thyroid gland predicted by the model is displayed as a mask to the CT image. Users can add or delete masks to complete thyroid segmentation (**Figure 8**).

The thyroid nodule was expressed as a circle, and the length of the radius was determined by clicking the center and dragging the mouse. In general, nodules often assume a roughly circular shape, so, as a rule, the drawing of nodules is performed on the image of the nodule with the largest diameter (**Figure 9**).

The “export to files” function stacks the modified masks, forms a 3D object according to the mesh-type 3D modeling technique, and obtains and outputs facet and vertex information of the reconstructed 3D thyroid gland model. Finally, the mesh structure is constructed from the facet and vertex information.

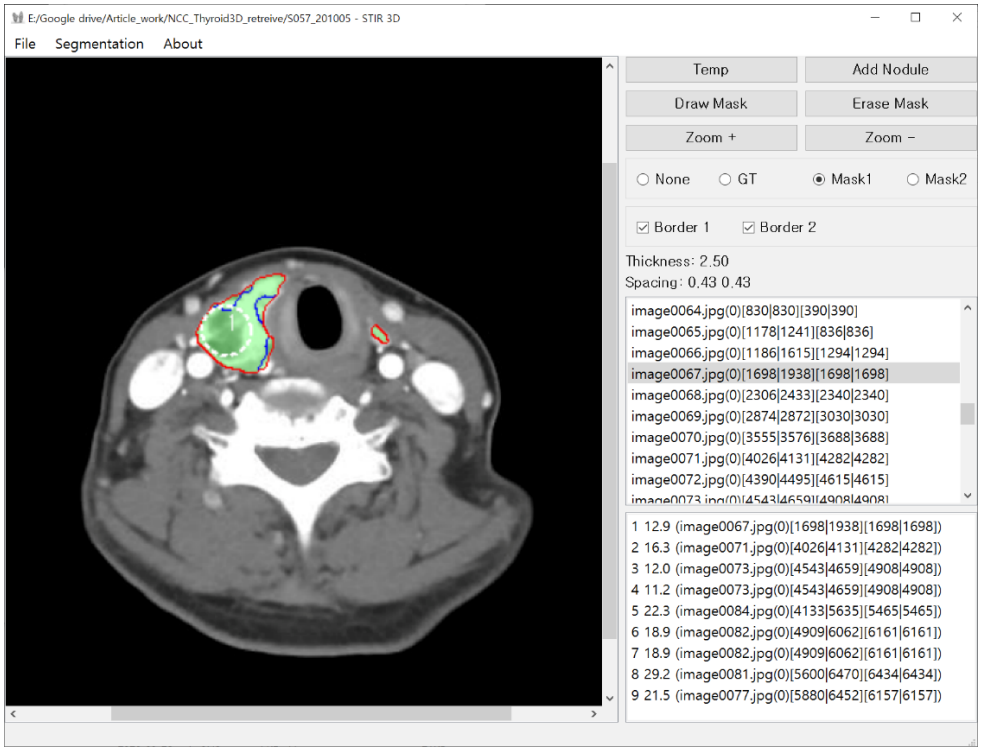
E:/Google drive/Article_work/NCC_Thyroid3D_retreive/S057_201005 - STIR 3D
File
Segmentation
About
Temp
Add Nodule
Draw Mask
Erase Mask
Zoom +
Zoom −
None
GT
Mask1
Mask2
Border 1
Border 2
Thickness: 2.50
Spacing: 0.43 0.43
image0064.jpg(0)[830|830][390|390]
image0065.jpg(0)[1178|1241][836|836]
image0066.jpg(0)[1186|1615][1294|1294]
image0067.jpg(0)[1698|1938][1698|1698]
image0068.jpg(0)[2306|2433][2340|2340]
image0069.jpg(0)[2874|2872][3030|3030]
image0070.jpg(0)[3555|3576][3688|3688]
image0071.jpg(0)[4026|4131][4282|4282]
image0072.jpg(0)[4390|4495][4615|4615]
1 12.9 (image0067.jpg(0)[1698|1938][1698|1698])
2 16.3 (image0071.jpg(0)[4026|4131][4282|4282])
3 12.0 (image0073.jpg(0)[4543|4659][4908|4908])
4 11.2 (image0073.jpg(0)[4543|4659][4908|4908])
5 22.3 (image0084.jpg(0)[4133|5635][5465|5465])
6 18.9 (image0082.jpg(0)[4909|6062][6161|6161])
7 18.9 (image0082.jpg(0)[4909|6062][6161|6161])
8 29.2 (image0081.jpg(0)[5600|6470][6434|6434])
9 21.5 (image0077.jpg(0)[5880|6452][6157|6157])

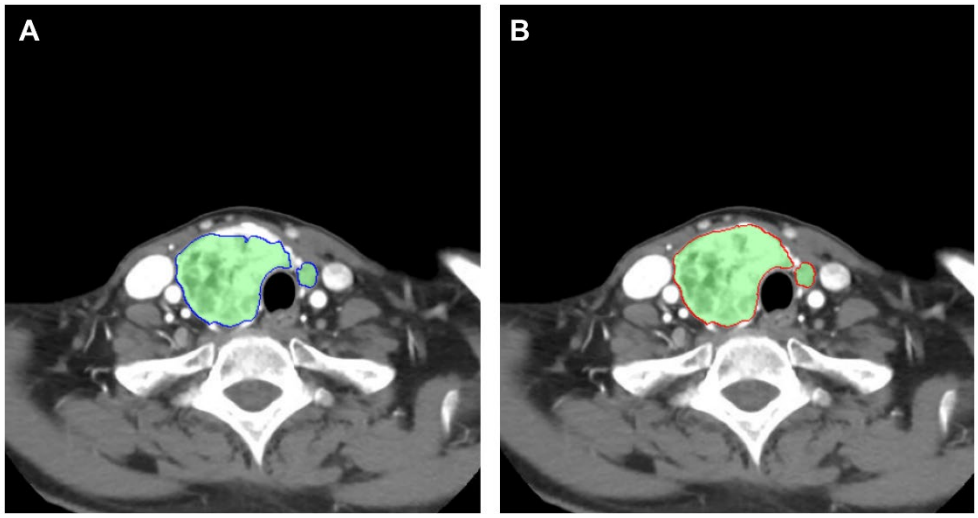
A
B

S

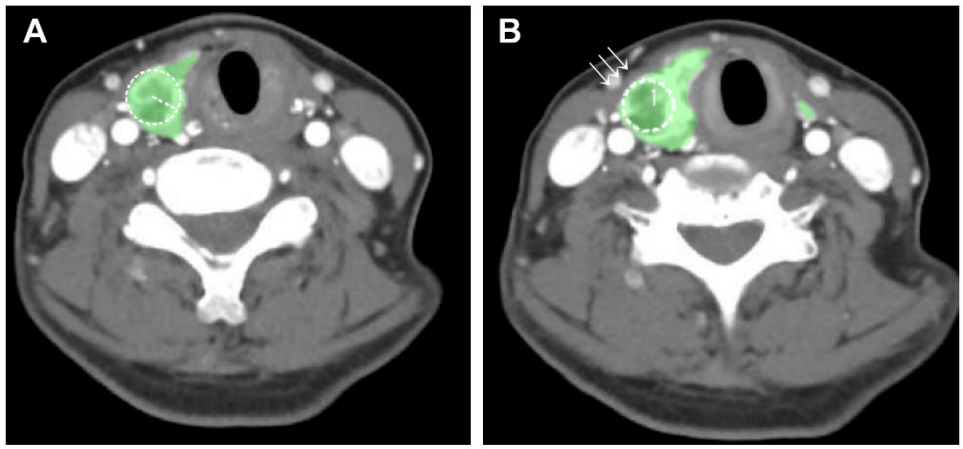
A
B

2.4. A Prospective Clinical Study using 3D Thyroid Gland Model

2.4.1. Purpose of the Prospective Clinical Study

The main purpose of the clinical study was to evaluate the usefulness of the 3D thyroid gland model for obtaining informed consent. To this end, the study was designed to assess the degree of patients' understanding of the disease and surgery, as well as their satisfaction level when using or not using the 3D thyroid gland model during the informed consent process. When the 3D thyroid gland model was not used, only a conventional method, such as an illustration and standardized anatomical models, was utilized.

2.4.2. Patients

Adults 18 years of age or older with an indication for thyroid gland surgery were eligible to participate in the study. The exclusion criteria included withdrawal from the study or cancellation of the surgery beforehand.

A total of 60 patients were consecutively enrolled from July to October 2020 (**Figure 10**). After enrollment, the patients were assigned into two groups by block-randomization rules, with a block size of four. A randomization list was created using R statistical software (version 3.5.1; R Foundation for Statistical Computing, Vienna, Austria) and administered by another investigator (SY) who did not meet the patient in person.

A personalized 3D thyroid gland model was fabricated before obtaining informed consent regardless of the patient's group allocation. On a patient-visiting day, the attending physician of each patient was notified of the study group in which the patient was enrolled for obtaining informed consent. The surgical procedure was explained to the patient according to the study group (i.e., with or without 3D thyroid gland model).

The first questionnaire administered to patients after obtaining informed consent was modified from that of Yoon et al. (**Table 2**) [10]. The questionnaire was comprised of four main categories (general knowledge, benefits of surgery, risks of surgery, and satisfaction). Each category contained three questions and each question was scored from 1 to 5, corresponding to strongly disagree, disagree, neutral, agree, and strongly agree, respectively.

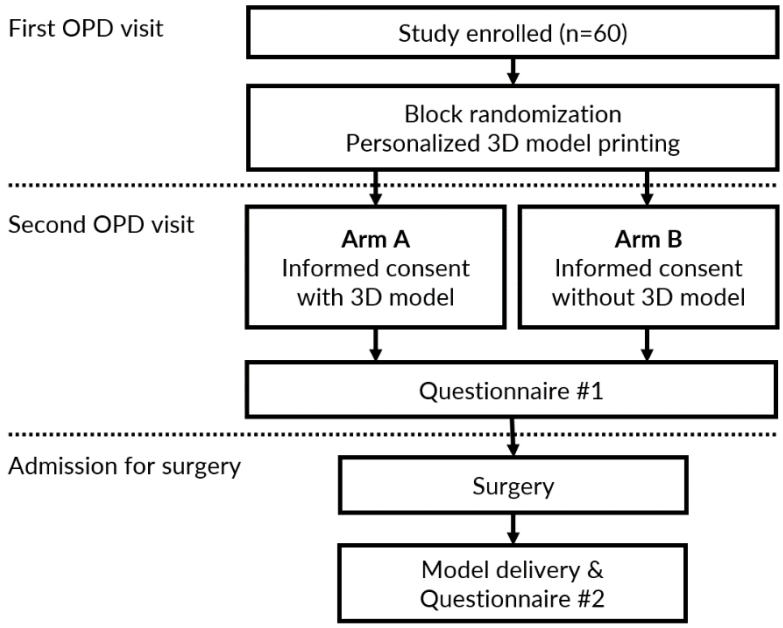

Inclusion criteria

- Adult patient (>18-year-old)
- Indication for thyroid surgery

Exclusion criteria (at any time)

- Withdrawal after enrollment
- Cancellation of surgery

Table 2. First questionnaire, administered immediately after obtaining informed consent with or without the 3D-printed thyroid gland model for thyroid surgery.

Questions*	1	2	3	4	5
General Knowledge					
1. I understand the location and size of thyroid lesion that will be surgically resected.	□	□	□	□	□
2. I understand the disease status of the thyroid lesion(s) (malignant/benign).	□	□	□	□	□
3. I understand the surgical procedure that will be performed.	□	□	□	□	□
Benefits					
4. I understand the purpose of the surgery.	□	□	□	□	□
5. I understand the extent of the surgery and its rationale.	□	□	□	□	□
6. I understand the expected survival and recurrence rates after treatment.	□	□	□	□	□
Risks					
7. I understand the potential complications related to the surgery.	□	□	□	□	□
8. I understand the possibility of a delayed discharge from the hospital due to complications or the need for additional treatment.	□	□	□	□	□
9. I understand that the potential complications may vary depending on the location and size of the lesion in relation to recurrent laryngeal nerve and blood vessels.	□	□	□	□	□
Satisfaction					
10. I am sufficiently informed about the surgery and satisfied with the explanation.	□	□	□	□	□
11. I am satisfied with my decision and the medical staff.	□	□	□	□	□
12. I am satisfied with my understanding of the disease.	□	□	□	□	□

* Rating: (1) strongly disagree, (2) disagree, (3) neutral, (4) agree, and (5) strongly agree.

After surgery, all patients were provided with their 3D thyroid gland models and asked to answer the second questionnaire, a shortened version of the first questionnaire. Patients rated how much their understanding and satisfaction were improved by their personalized 3D-printed thyroid gland model, from 1 to 5 (strongly disagree, disagree, neutral, agree, and strongly agree). If multiple questions shared the highest ratings of improvement among the four questions, the patients were asked to choose only one of them (**Table 3**).

Basic information on age, gender, pathological diagnosis, pathological TNM classification, and operation type (extent) were collected. Information on social status and past medical history assessed at the time of admission for surgery were also collected. All patients were operated on by one of four thyroid surgeons (JS, CHR, YSJ, and JR) who share a common policy on indication and extent for surgery.

Preoperatively, all patients were subjected to ultrasonography and CT scanning, which are routinely applied in the institute. When CT had been performed in other institutions, patients did not require an additional CT scan because all DICOM files contained information on slice thickness and pixel spacing.

Table 3. Second questionnaire, administered immediately after surgery and providing the personalized 3D-printed thyroid gland model.

Questions*	1	2	3	4	5
1. The personalized 3D-printed thyroid gland model enhanced my understanding of my thyroid disease (cancer/nodule).	□	□	□	□	□
2. The personalized 3D-printed thyroid gland model enhanced my understanding of the rea-son, extent, and procedure of the surgery.	□	□	□	□	□
3. The personalized 3D-printed thyroid gland model enhanced my understanding of the possible complications and adverse results of the surgery.	□	□	□	□	□
4. The personalized 3D-printed thyroid gland model enhanced my satisfaction with the clinicians and institution.	□	□	□	□	□
If the highest degree of improvement was more than two, which of the items do you think is the most helpful? (Items 1–4)	1. □ 2. □ 3. □ 4. □				

* Rating: (1) strongly disagree, (2) disagree, (3) neutral, (4) agree, and (5) strongly agree.

2.4.3. 3D Model Reconstruction and 3D Printing

The 3D thyroid gland model reconstruction and correction of the inference using the deep learning model for all patients was carried out using the STIR 3D application.

All STL files were printed using a 3DWOX 2X printer by a single engineer (SY) in the same manner as the initial mesh-type 3D printing experiment. The 3D printing time and post-processing time were checked. The cost was measured by calculating the amount of filament used, excluding labor costs.

2.4.4. Statistical Analysis

Statistical analysis was performed using R statistical software. The sample size was determined by using the *pwr* package to detect an absolute difference of 20% between two groups for the increase or decrease of scores with 80% power, while the type I error (two-sided) was set at 5% [35]. Two groups were assumed to have a standard deviation of 25% of the mean value, and a 15% dropout rate was considered. Therefore, 30 patients were allocated to each group.

The average score for each questionnaire was compared using Welch's t-test because the two groups had unequal final sample sizes.

To evaluate the accuracy of the deep learning model during the prospective study, the area initially inferred by the deep learning model was compared with the manually corrected area. Since there was no pre-annotated ground truth in the prospective study, in contrast to the training of the deep learning model, the area after manual correction was regarded as the ground truth. Accordingly, if the initial inference of the deep learning model was not changed, the Dice coefficient was calculated as 1.000.

2.4.5. Ethical Considerations

During the prospective study, all participants provided written informed consent according to the policies and procedures approved by the IRB of the same institute (No. NCC2019-0256). The study was registered on cris.nih.go.kr (Identifier: KCT0005069).

Chapter 3. Results

3.1. Mesh-Type 3D-Printed Model of Human Organ-Tumor Model

Six organ-tumor models were printed using a mesh-type 3D printing method (**Figure 11**). Adjacent structures were distinguishable based on their different mesh densities, as follows: thyroid lobe and trachea (**Figure 11C**), maxillary bone and teeth (**Figure 11D**), breast and nipple (**Figure 11E**), and the three lobes of the right lung (**Figure 11F**). The mesh style is indicative of tumor occupancy in 3D (even if inside solid organs), without the need for transparent material. The printed dimensions (relative to actual size), printing time, post-processing time, and cost were evaluated in each organ-tumor model (**Table 4**). Both printing time and cost were significantly correlated with the 3D model size (1.73 min/cm^3 and \$0.05 USD/cm^3, $p < .001$).

Figure 12 shows a 3D-printed model of a thyroid gland compared with the actual thyroidectomy specimen. No disparities in glandular size or contour were observed. The model and surgical specimen also corresponded well in terms of tumor location.

This 3D visualization technique for tumor localization was registered as a Republic of Korea patent (No. 10-2227735; filed on January 3, 2020; registered on March 9, 2021).

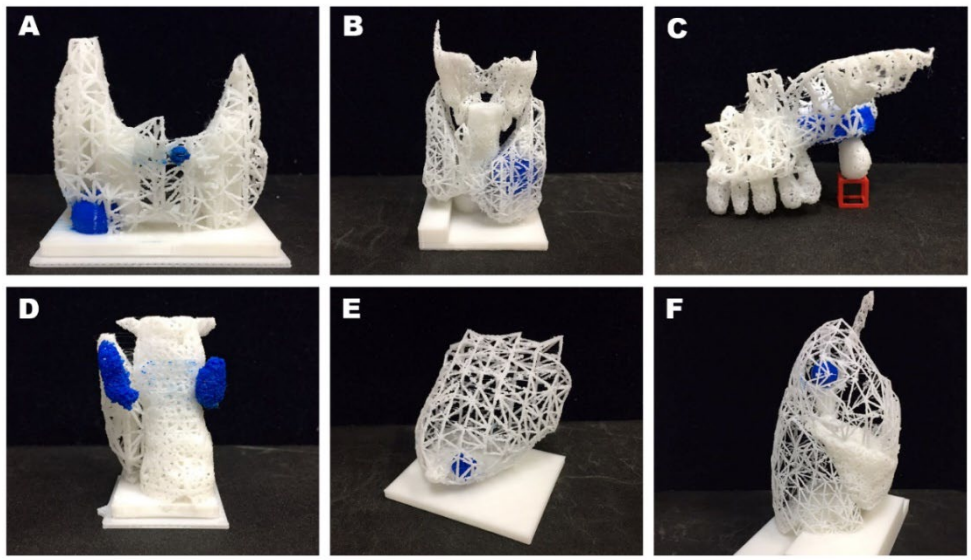

Figure 11. Examples of mesh-type 3D modeling: tumors of thyroid gland (A); thyroid gland and adjacent cartilage (B); maxillary tumor (lateral view) (C); parathyroid adenoma (posterior view) (D); breast tumor (E); and right lung nodule (lateral view) (F). Note: each tumor is printed in blue; the different mesh densities of the adjacent structures are also shown. This figure has been reproduced with permission from the publisher.

Table 4. Specifications, production times, and costs of various mesh-type 3D models. This table has been reproduced with permission from the publisher.

Model	Size (cm)	Ratio to Actual size	Printing Time	Post-processing Time (min)	Cost
Thyroid tumor	5.3 × 3.0 × 6.5	1	2 h 50 m	10	$2.72
Thyroid gland and adjacent cartilage	5.5 × 4.3 × 9.3	1	9 h 15 m	10	$8.69
Maxillary tumor	7.1 × 5.7 × 4.7	1	9 h 4 m	15	$8.24
Parathyroid adenoma	4.0 × 3.1 × 5.5	1	5 h 3 m	10	$3.71
Breast tumor	6.2 × 5.2 × 5.9	½	6 h 41 m	5	$7.78
Lung nodule	6.8 × 8.0 × 13.5	½	23 h 4 m	40	$33.67

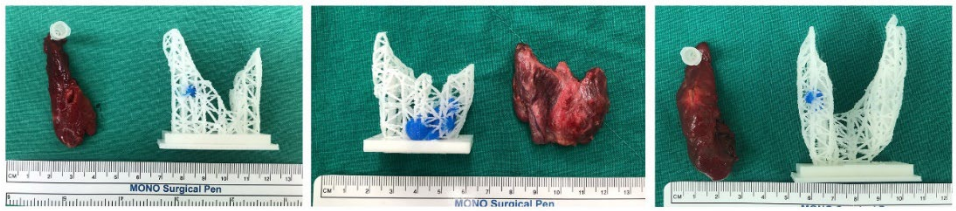

Figure 12. Side-by-side comparison of a 3D-printed thyroidal prototype and corresponding surgical specimen. This figure has been reproduced with permission from the publisher.

3.2. Deep learning Model for Thyroid Segmentation

The deep learning model achieved the highest-validation Dice coefficient at the 625th Epoch (0.932 in the training set, 0.944 in the validation set, and 0.894 in the test set) (**Figure 13**).

During the prospective study, a total of 53 CT series from the enrolled patients were inferred by the deep learning model. The average Dice coefficient was 0.976, which was higher than that obtained from the deep learning training set (training set: 0.932; validation set: 0.944; and test set: 0.894) (**Table 5**). Sample images illustrating how the deep learning model inferred the thyroid area are presented in **Figure 14-17**.

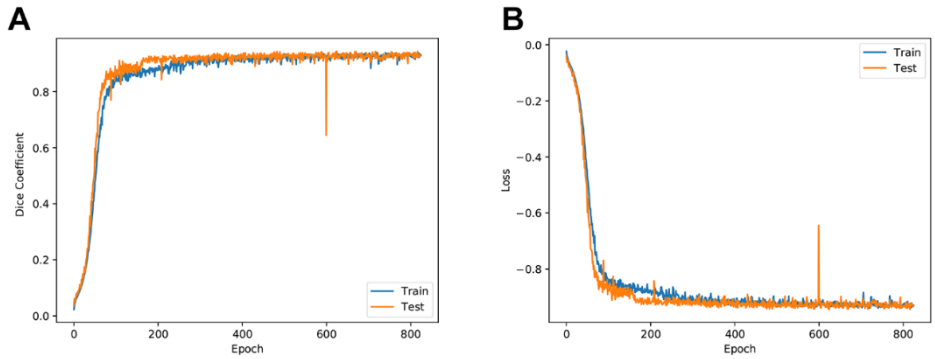

Figure 13. Change in Dice coefficient according to deep learning model training (A) and change of loss value defined as -1 * Dice coefficient (B).

Table 5. Log data for the 53 patients enrolled in the study.

Serial No.	CT protocol	Dice coefficient	Editing time for segmentation (min)	3D printing time (min)	Post-processing time (min)	Price ($)
S003	Thyroid CT	0.999	2	134	5	2.44
S004	Thyroid CT	1.000	2	181	10	3.41
S007	Thyroid CT	0.790	10	330	5	5.17
S008	Thyroid CT	0.993	4	225	5	5.17
S009	Thyroid CT	0.966	3	186	5	3.90
S010	Thyroid CT	0.967	6	206	5	4.39
S012	Thyroid CT	0.986	3	177	5	2.15
S013	Thyroid CT	0.981	3	303	5	7.41
S014	Thyroid CT	0.922	6	151	5	2.83
S015	Thyroid CT	0.910	18	393	5	6.73
S016	Thyroid CT	0.993	3	174	5	3.32
S017	Thyroid CT	0.985	4	237	5	3.32
S019	Thyroid CT	0.968	3	220	5	3.80
S020	Thyroid CT	0.894	18	388	5	7.90
S021	Thyroid CT	0.983	3	230	5	2.93
S022	Thyroid CT	0.966	3	151	5	3.22
S023	Thyroid CT	0.982	3	158	5	3.02
S024	Thyroid CT	0.991	4	220	5	4.19
S025	Thyroid CT	0.948	5	266	5	4.00
S026	Thyroid CT	0.997	2	213	5	2.73
S027	Thyroid CT	0.980	4	215	5	4.09
S028	Thyroid CT	0.991	3	200	5	2.34
S029	Thyroid CT	0.994	2	249	5	3.51
S030	Thyroid CT	0.997	2	214	5	4.49
S031	Thyroid CT	0.998	2	220	5	5.17
S032	Thyroid CT	0.968	4	287	5	3.61
S033	Thyroid CT	0.999	2	150	5	2.73
S034	Thyroid CT	0.984	2	275	5	4.29
S035	Thyroid CT	0.941	6	284	5	5.27
S036	Thyroid CT	0.996	2	202	5	2.34
S037	Thyroid CT	0.993	2	231	5	3.12
S038	Thyroid CT	0.996	3	223	5	2.93
S039	Thyroid CT	0.961	6	424	15	7.51
S040	Thyroid CT	0.989	3	225	5	2.73
S041	Thyroid CT	0.985	2	410	10	4.29
S042	Thyroid CT	0.995	2	332	5	4.88
S043	Thyroid CT	1.000	1	231	5	2.63
S044	Thyroid CT	0.995	3	236	5	2.93
S045	Thyroid CT	0.987	2	304	5	5.27
S046	Thyroid CT	1.000	2	189	5	3.61
S047	Outside (contrast)	0.965	4	335	5	5.17
S048	Outside (contrast)	0.889	11	420	10	8.39
S049	Outside (contrast)	0.993	4	282	5	3.61
S050	Thyroid CT	0.998	2	200	5	2.15
S051	Thyroid CT	1.000	1	258	5	2.83
S052	Thyroid CT	0.985	3	265	5	4.10

S054	Thyroid CT	0.994	3	342	5	5.17
S055	Thyroid CT	0.993	3	395	10	7.02
S056	Thyroid CT	1.000	2	218	5	3.61
S057	Thyroid CT	0.927	14	188	5	8.88
S058	Thyroid CT	0.994	3	256	5	3.71
S059	Thyroid CT	0.998	3	423	5	7.32
S060	Thyroid CT	1.000	1	203	5	2.63

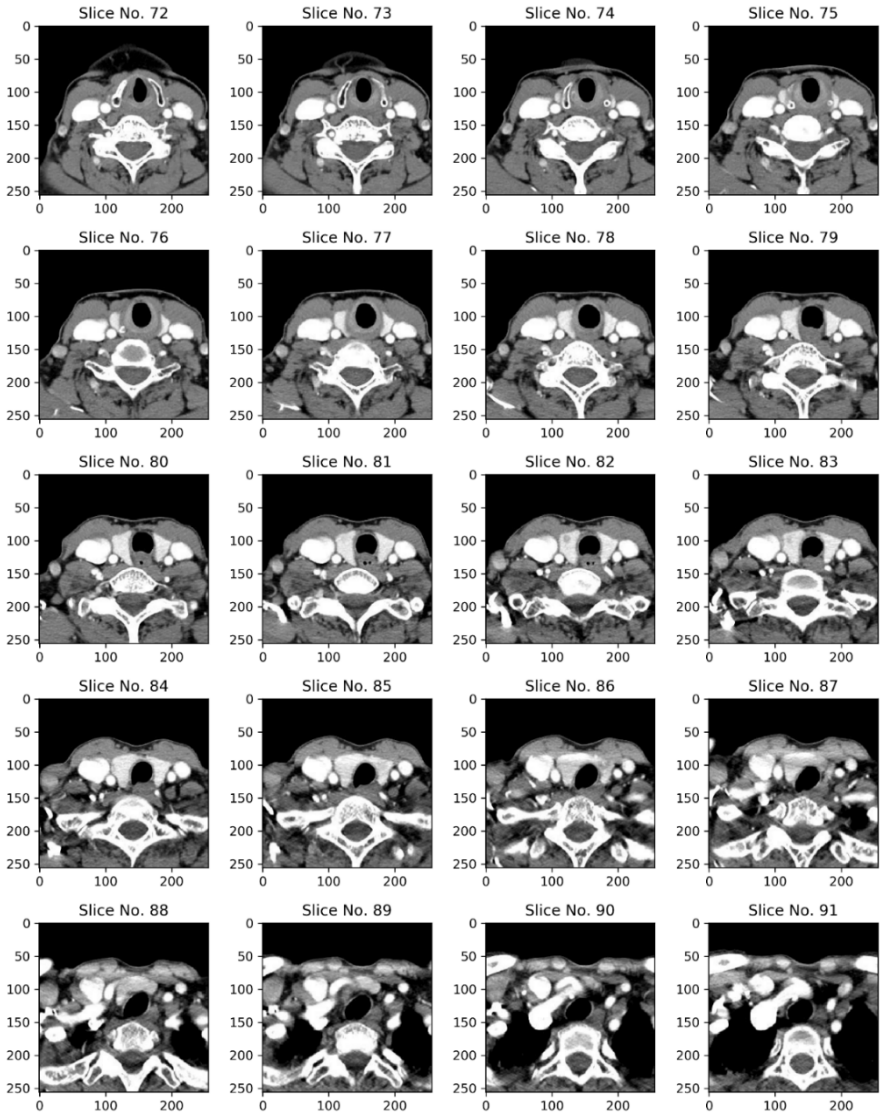

Figure 14. Original Thyroid CT images (slices 72–91) for patient S004.

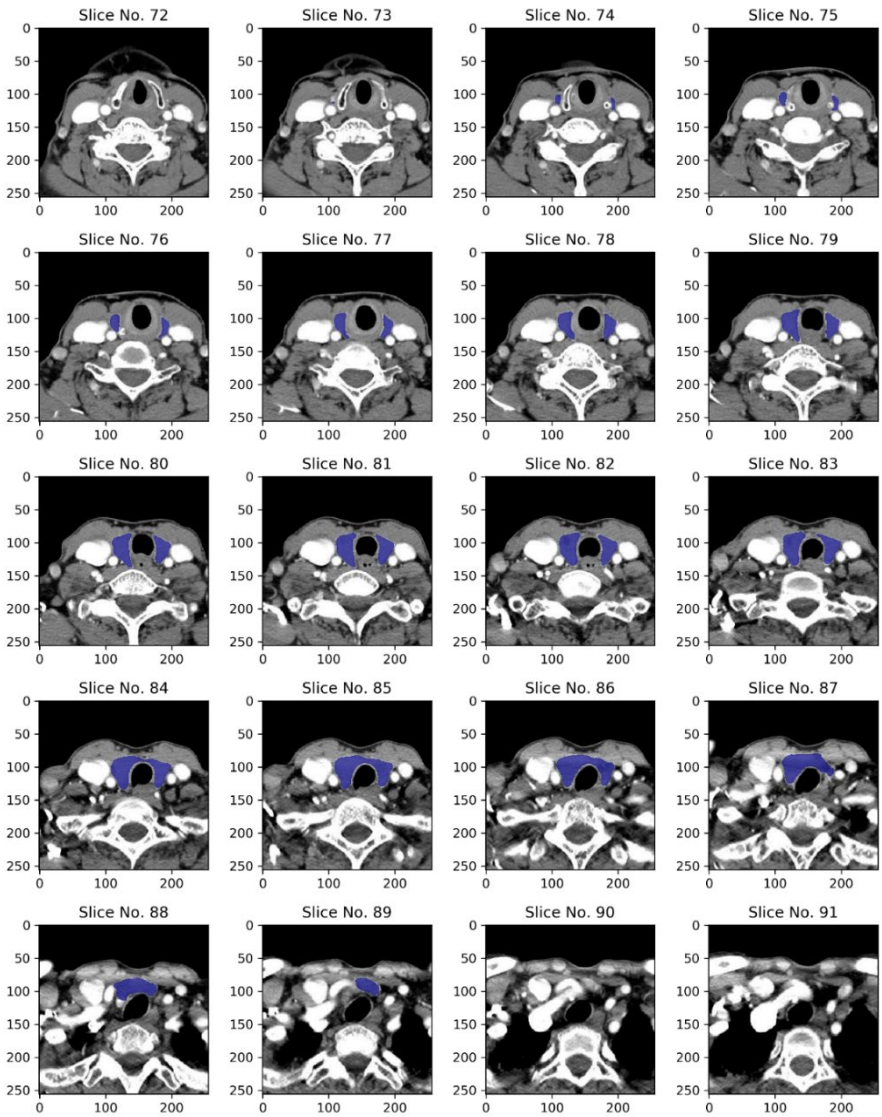

Figure 15. Segmentation results for the CT slices of patient S004. The blue mask is the area segmented by the deep learning model. The Dice similarity coefficient was 1.000 and required no correction. Segmentation was successfully achieved in slices where the thyroid gland was observed.

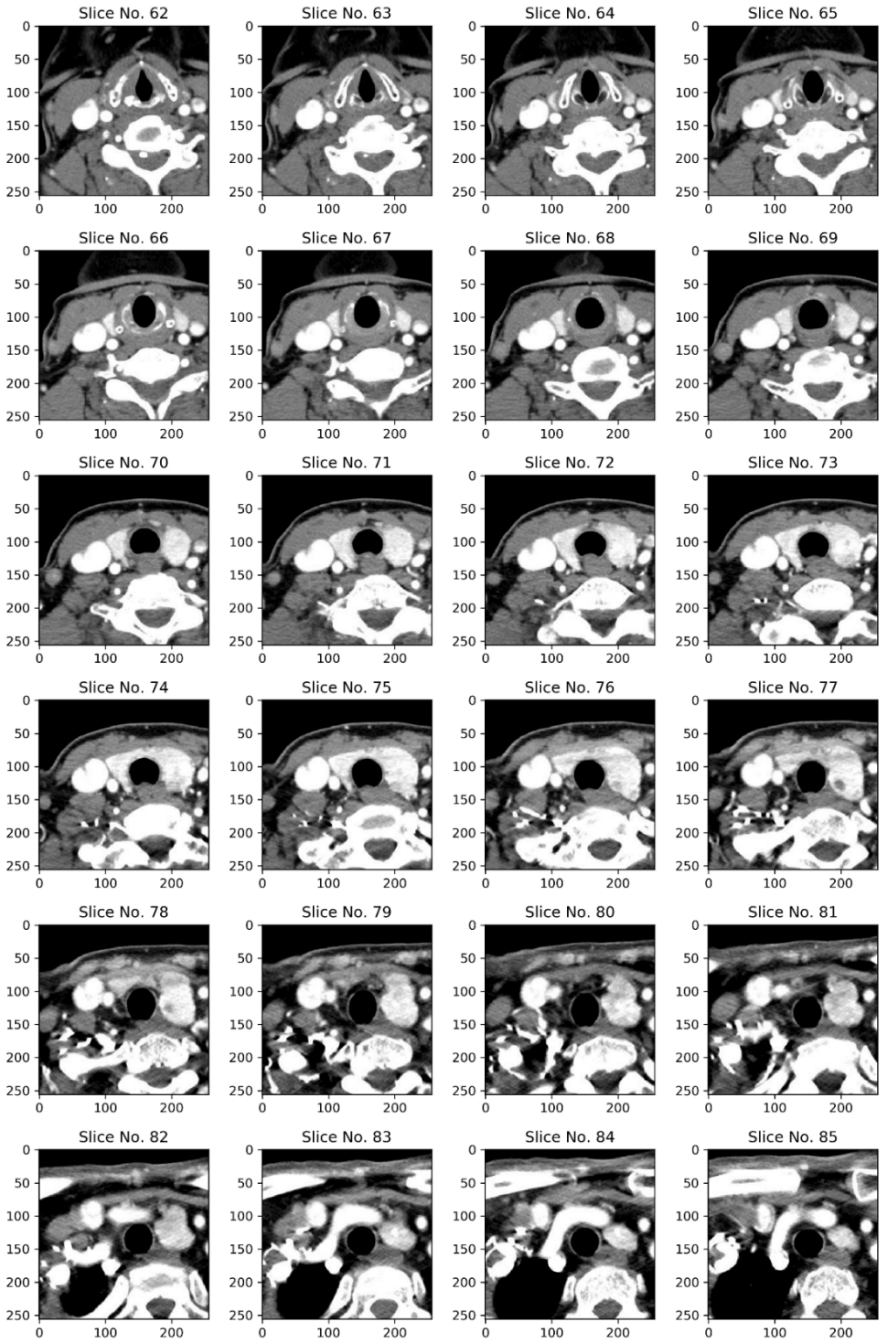

Figure 16. Original thyroid CT images (slices 62–85) for patient S007. The patient has an enlarged left thyroid.

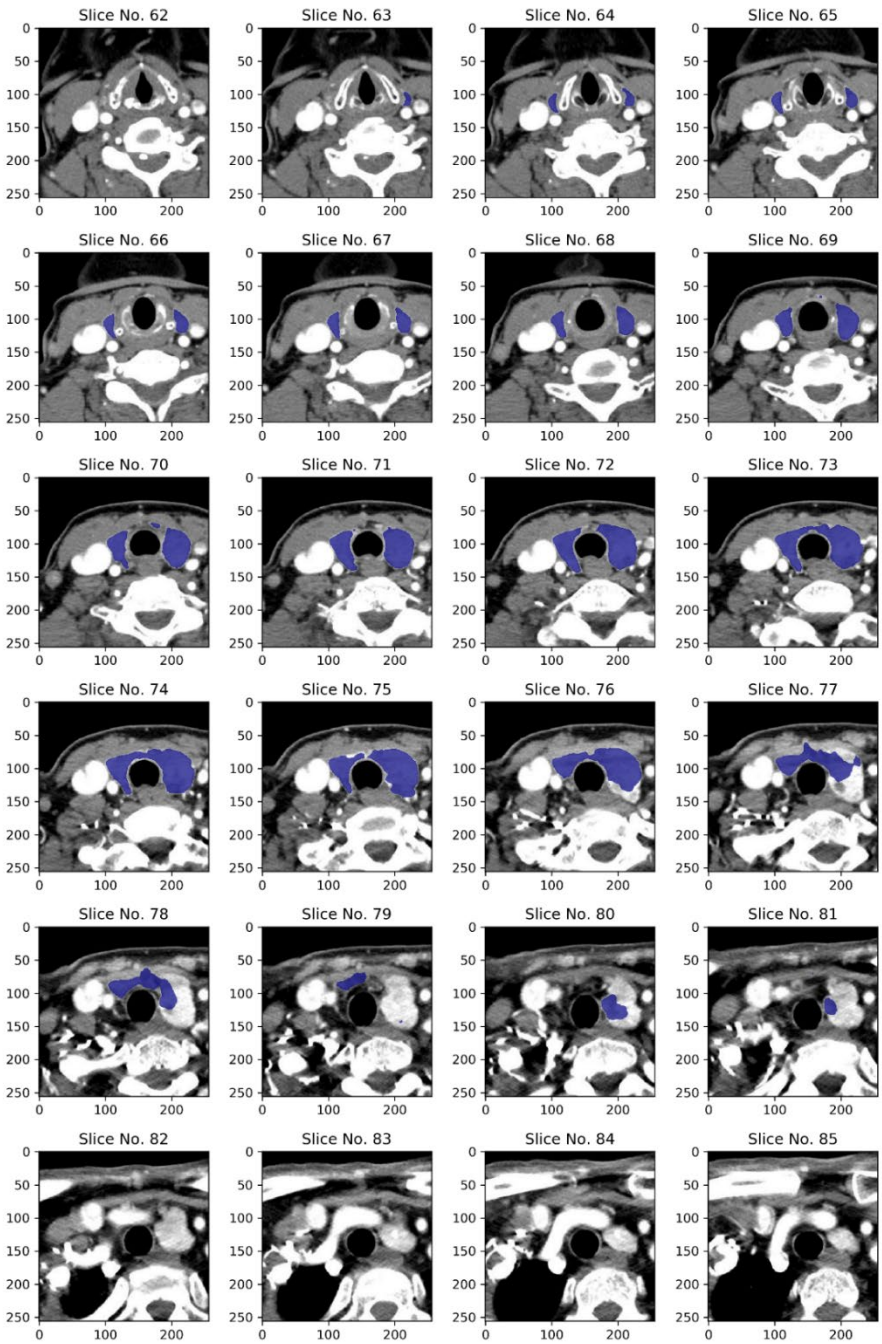

Figure 17. Segmentation results for the CT slices of patient S007. The blue mask is the area segmented by the deep learning model. The Dice similarity coefficient was 0.790, which represents the lowest accuracy. From the 76th slide, the goitrous left thyroid lobe was not completely segmented.

3.3. Prospective Study on Obtaining Informed Consent

3.3.1. Demographics and 3D Thyroid Gland Model Production

Of the 60 enrolled patients, seven were excluded owing to either a delay or cancellation of surgery. The number of patients included in the study consisted of 28 who provided informed consent for the use of a personalized 3D-printed model and 25 who provided informed consent with conventional tools (**Table 6**). Age, sex, diagnosis, pathological diagnosis, pathological T (pT) and N (pN) classification, and operation methods were not significantly different between the two groups. Three of the 53 patients received CT scans at other institutions. The social status and medical history of the enrolled patients are shown in **Table 7**.

For the 53 patients who finished the study, all mesh-type 3D model reconstructions using deep learning and 3D printing were completed without any issues. The mean editing time to correct the inferred area of the images using the STIR 3D application was 4.0 min (standard deviation [SD]: 3.7, min to max: 1–18), and the mean total 3D printing time was 258.9 min (SD: 78.8, min to max: 139–439). The mean price for producing the 3D-printed models was USD 4.23 (SD: 1.71, min to max: 2.15–8.88) (**Table 5**).

The 3D models were compared to the actual surgical specimens and were found to match in terms of the approximate size and location of the lesions (**Figure 18**). For the two cases of patients with cT3bN1b who underwent a total thyroidectomy, one was suspected to have an anterior external thyroidal extension, and the other was diagnosed with a posterior external thyroidal extension in the upper pole based on preoperative CT and ultrasonography. The 3D models reflected each external thyroidal extension based on the preoperative evaluation. Surgery confirmed them as intraglandular tumors; however, the location and size of the lesions were consistent between the surgical specimens and 3D-printed models (**Figure 19**).

Table 6. Demographics of the enrolled patients. This table has been reproduced with permission from the publisher.

		With 3D Model (n = 28)	**With Conventional Tools (n = 25)**	***p***
Age		49.2 ± 11.3	42.4 ± 15.8	.083*
Sex	Female	24 (85.7%)	18 (72.0%)	.313†
	Male	4 (14.3%)	7 (28.0%)	
Pathological Diagnosis	Malignant §	25 (89.3%)	25 (100.0%)	.238†
	Benign	3 (10.7%)	0 (0.0%)	
pT Classification‡	1	21 (84.0%)	19 (76.0%)	.615†
	2	0 (0.0%)	2 (8.0%)	
	3	4 (16.0%)	4 (16.0%)	
	4	0 (0.0%)	0 (0.0%)	
pN Classification‡	0	13 (52.0%)	15 (60.0%)	.639†
	1a	6 (24.0%)	7 (28.0%)	
	1b	6 (24.0%)	3 (12.0%)	
Operation	Lobectomy	18 (64.3%)	13 (52.0%)	.413†
	Total thyroidectomy	10 (35.7%)	12 (48.0%)	

Abbreviations: pT, pathological T; pN, pathological N; * Welch's t-test; † Fisher's exact test; ‡ The number of pT and pN classifications were only for malignant cases; § One case of follicular thyroid carcinoma was included in the group without the 3D model; otherwise, the tumors were papillary thyroid carcinoma.

Table 7. Social status and medical history of the enrolled patients (n = 53).

Cohabitation status	
Cohabitant	45 (84.9%)
Alone	8 (15.1%)
Education	
University or higher graduate	28 (52.8%)
Secondary school or lower graduate	25 (47.2%)
Employment	
Employed	35 (66.0%)
Unemployed	17 (32.1%)
Full-time student	1 (1.9%)
Religion observer	
Yes	21 (39.6%)
No	32 (60.4%)
Smoking	
Active	1 (1.9%)
Ex-smoker	6 (11.3%)
Never	46 (86.8%)
Physical status	
ASA ≤ 2	53 (100.0%)
ASA ≥ 3	0 (0.0%)
Family history of thyroid cancer	
Yes	6 (11.3%)
No	47 (88.7%)
Previous surgery, including surgery with local anesthesia	
Yes	36 (69.8%)
No	17 (30.2%)

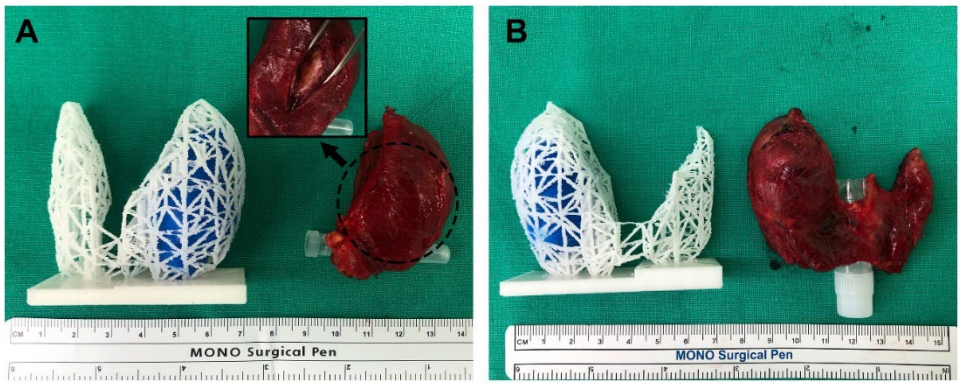

Figure 18. Comparison of the 3D models and actual surgical specimens (A, B). As shown in the 3D models, both cases are intraglandular tumors, similar to the thyroid gland in terms of size and shape. This figure has been reproduced with permission from the publisher.

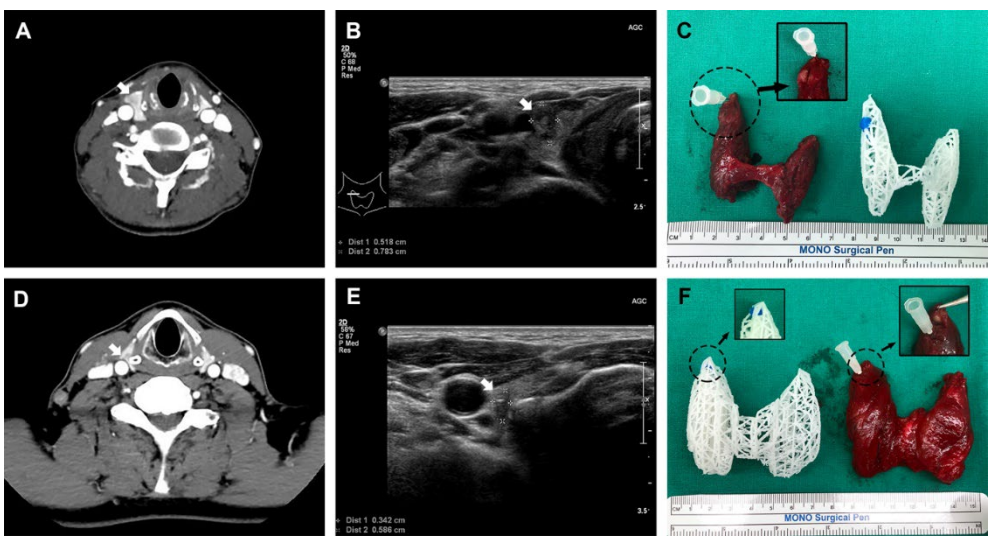

Figure 19. Two total thyroidectomized cases, which were clinically cT3bN1b. Based on the preoperative CT and ultrasonography results, each case exhibited anterior (A–C) and posterior (D–F) external thyroidal extension into the upper pole, respectively (white arrow indicates thyroid cancer). This figure has been reproduced with permission from the publisher.

3.3.2. Results of the First Questionnaire

The first questionnaire was given to patients immediately after obtaining informed consent. As a result, the ratings for 8 of the 12 items were significantly improved when using personalized 3D-printed models compared to using the conventional method (**Table 8**). After dividing the questionnaire into four major categories (general knowledge, benefits of surgery, risks of surgery, and satisfaction), the group presented with 3D-printed models gave significantly higher ratings in all categories than the group provided with the conventional explanation (14.1 ± 1.2 vs. 12.8 ± 1.8 for the general knowledge, $p = .005$; 14.1 ± 1.2 vs. 13.1 ± 1.6 for benefits, $p = .016$; 13.5 ± 1.7 vs. 12.5 ± 1.6 for risks, $p = .026$; 14.2 ± 1.2 vs. 13.4 ± 1.4 for satisfaction, $p = .036$) (**Figure 20**).

3.3.3. Results of the Second Questionnaire

After surgery and receiving their 3D-printed thyroid gland model, none of the patients indicated that their understanding or satisfaction were worsened by the 3D-printed model. The answers to all four questions were either “agree” or “strongly agree”; the questions related to understanding the disease and overall satisfaction were rated significantly higher than that asking participants to gauge their understanding of the possible complications ($p = .010$ and .044, respectively) (**Figure 21A**). Among individual patients, 38 (71.7%) chose “understanding the disease,” nine (17.0%) chose “overall satisfaction,” and six (11.3%) chose “understanding the operation” as the highest-rated item (**Figure 21B**).

Table 8. Detailed results of the first questionnaire.

	With 3D Model (n = 28)	**With Conventional Tools (n = 25)**	***p****
General Knowledge			
1. I understand the location and size of thyroid lesion that will be surgically. resected	4.6 ± 0.6	4.3 ± 0.6	.095
2. I understand the disease status of the thyroid lesion(s) (malignant/benign).	4.8 ± 0.4	4.3 ± 0.6	.002
3. I understand the surgical procedure that will be performed.	4.7 ± 0.5	4.2 ± 0.7	.007
Benefit			
4. I understand the purpose of the surgery.	4.6 ± 0.6	4.5 ± 0.5	.234
5. I understand the extent of the surgery and its rationale	4.8 ± 0.4	4.4 ± 0.6	.004
6. I understand the expected survival and recurrence rates after treatment.	4.6 ± 0.6	4.2 ± 0.7	.026
Risk			
7. I understand the potential complications related to the surgery.	4.5 ± 0.6	4.0 ± 0.6	.006
8. I understand the possibility of a delayed discharge from the hospital due to complications or the need for additional treatment.	4.4 ± 0.7	4.3 ± 0.6	.332
9. I understand that the potential complications may vary depending on the location and size of the lesion in relation to recurrent laryngeal nerve and blood vessels.	4.5 ± 0.6	4.1 ± 0.6	.018
Satisfaction			
10. I am sufficiently informed about the surgery and satisfied with the explanation.	4.7 ± 0.4	4.5 ± 0.5	.057
11. I am satisfied with my decision and the medical staff.	4.7 ± 0.6	4.5 ± 0.5	.142
12. I am satisfied with my understanding of the disease.	4.8 ± 0.4	4.4 ± 0.5	.014

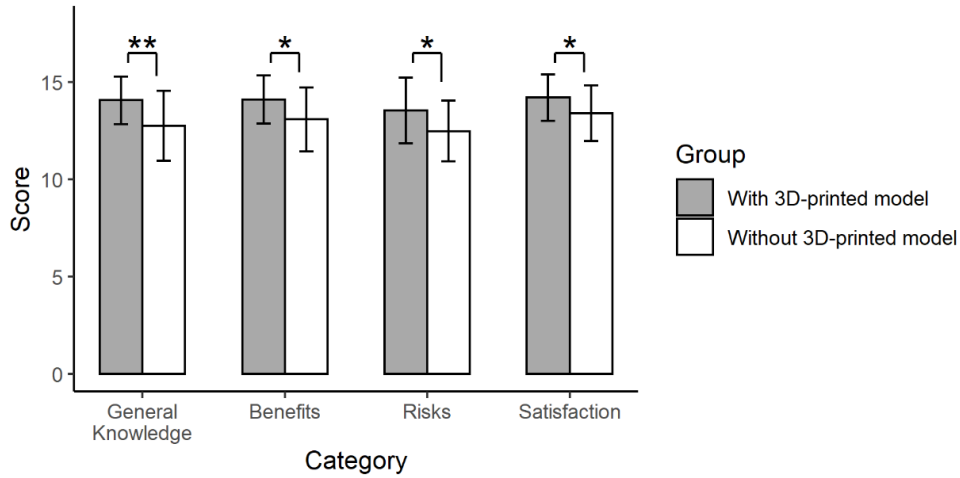

Figure 20. Results of the first questionnaire. Twelve items were grouped into four categories (general knowledge, benefits of surgery, risks of surgery, and satisfaction) (**, $p < .01$; *, $p < .05$). This figure has been reproduced with permission from the publisher.

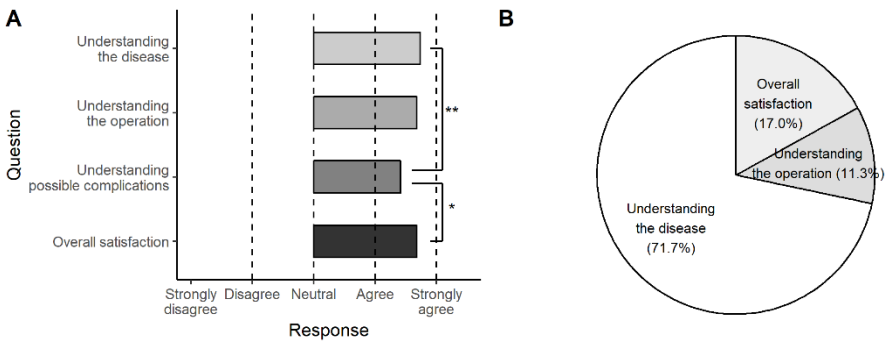

Figure 21. Results of the second questionnaire. The 3D-printed model was helpful in all categories (A) and most effective in understanding the disease (71.7%) (B) (**, $p < .01$; *, $p < .05$). This figure has been reproduced with permission from the publisher.

Chapter 4. Discussion

4.1. Mesh-Type 3D Modeling Technique for Tumor localization

For head and neck oncology, tumor localization is important so that the surgeon may choose the surgical approach, decide the surgical extent, and prepare for possible complications. For example, in thyroid cancer with tracheal invasion, the degree to which the tumor has extended into the trachea is an important criterion for choosing between tracheal end-to-end anastomosis and wedge resection; the former procedure may have more fatal complications. As many important anatomical structures are gathered in the head and neck, tumor visualization therein may have more clinical utility than in any other surgical site.

One area where tumor localization may be used is in obtaining informed consent. For a positive doctor-patient relationship, an adequate amount of information conveyed to a competent patient provides a sound basis for voluntary and rational decision-making [36]. Therefore, patient-specific tumor visualization may facilitate physicians to achieve the primary goal of informed surgical consent by better conveying key surgical principles, including organ anatomy, local physiology, attributes, tumor location, and potential operative complications [9].

In portraying a solid tumor, capsular breech and invasion of surrounding tissues are other important considerations that a 3D model effectively addresses. A personalized model rendered by a 3D printer reinforces the mutual sense of awareness needed between patient and physician [9]. Although only a few studies to date have tested 3D models in patients facing thoracic, kidney, or orthopedic surgeries, they have consistently shown improved preoperative understanding or satisfaction [9-11]. Still, a number of issues pertaining to cost, resolution, and duration of printing and material texture must be resolved before 3D-printed models become more mainstream [12].

The novel methodology introduced here offers several advantages. The customary segmentation of targeted objects entailed in 3D reconstruction of tomographic images is readily applicable to mesh-type 3D modeling. Hence, newer CT systems are not required, and routine CT protocols for specific organs may be utilized. Likewise, an expensive 3D printer is not essential. Even if only two colors are available, tumors and normal structures can be

printed in different colors, and the density of the same color can be changed to differentiate two or more normal structures. In addition, tumors may be printed in either solid or mesh forms. Solid replicas may provide better visibility of small lesions. Filament requirements (and thus costs) are similarly reduced because the printed organs are largely empty inside. Given a magnitude of ≤10 cm, most models were fabricated within half a day. Thus, the day after CT or MRI studies were carried out, completed models were feasible. This 3D visualization technique for tumor localization was registered as a Republic of Korea patent in recognition of its novelty, non-obviousness, and utility.

There is some concern that mesh-type 3D modeling results do not accurately reflect the organs or tumors they represent. However, further attempts at refinement may nevertheless impose unwanted steps. For example, CT imaging using a 1 mm slice thickness (vs. routine setting) as a means of enhancing replication demands higher radiation exposure. Although not statistically proven, the size and contour of a printed thyroid gland and the tumor situated within it satisfactorily mimicked the attributes of the corresponding surgical specimen, confirming this approach as a viable tool for personalized care. However, for applications requiring narrower margins of error (i.e., as a surgical guide), the precision of specimen renderings should be studied.

With regard to study limitations, the PLA output is clearly of low quality, indicating a lack of sophistication [37]. In addition, the printing time of the mesh-type 3D models may be longer than that of the same volume of solid model with the same FDM printer; even half-size printing of a large organ (such as a lung) required nearly an entire day. However, reducing mesh density along with STL file reduction (decimation) could save printing time. Stringing may also develop as a technical issue, although this is avoidable by controlling the printer settings or resorting to non-FDM 3D-printing techniques.

Internally filled models (delineating tumors) for comparing costs and printing times were not fabricated because no transparent or translucent PLA filament was compatible with the printer. Overall, the mesh-type 3D model depicts the actual organ size and tumor location at low levels of resolution. This study remained focused on the modeling technique and its clinical translation, but a change in the default parameter settings might improve the resolution of the models. The optimal settings may even be organ specific. Moving forward, these are lingering issues to resolve. To truly establish the merits of mesh-type 3D modeling, further research is needed.

4.2. Prospective Study for Obtaining Informed Consent for Thyroid Gland Surgery

The surgical procedures for thyroid disease are relatively standardized (i.e., lobectomy or total thyroidectomy). However, the extent of surgery is decided by a comprehensive assessment of factors including tumor size (micro- or macro-), location (lobe or isthmus), invasion into surrounding tissue, and patient preference [38]. In other words, when the need for a lobectomy or total thyroidectomy is inconclusive, a patient's preference could dictate the approach. Therefore, providing patients with sufficient knowledge of their disease may be the most important part of the surgical decision. In this regard, the thyroid gland may be an appropriate organ for which to implement patient-specific 3D-printed models for enhancing a patient's understanding of their disease and treatment.

4.2.1. Fabrication of Personalized Thyroid 3D-Printed Model

The thyroid gland is a soft tissue organ; therefore, the degree of contrast enhancement varies significantly from patient to patient. The window level and width cannot be set similarly to when imaging hard tissue. A solution to this issue is region segmentation using a deep learning technique.

U-Net, a widely used deep learning architecture for semantic segmentation, was used as a backbone [34]. Although the dataset consisted of only 106 CT series, the Dice coefficient of approximately 0.9 was achieved by using image augmentation in the process of training. Interestingly, the deep learning model outperformed in the prospective study compared to the training process. The reason was that the Dice coefficient while training was calculated using the annotated area, which was determined by a physician without any previous information, as the ground truth. In contrast, the Dice coefficient for the prospective study was calculated using the post-processed segmentation area as the ground truth; however, post-processing was performed after the physician referred to the inference of the deep learning model. As each anatomical structure in the CT or MRI image may have low contrast with the adjacent organs [39,40], some of the errors in the inferenced segmentation may be tolerated based on the clinician's judgment, and eventually this discrepancy might lead to improved performance in the prospective study.

This study is meaningful as an actual case of using deep learning as software. During the final stages of the inference by artificial intelligence, medical staff intervened and used the software to complete the results. The software saved the staff's time by replacing the monotonous and inconvenient task of segmenting the thyroid gland on every CT slice. This proves that deep learning, which has shown promising results, can save time and has practical usability in medical applications.

Using a commercially available two-color 3D printer (approximately USD 5,000 in the Republic of Korea), all 3D models were printed without any issues. The mean total 3D printing time was 258.9 min, and the mean price for production was USD 4.23. Although labor cost was excluded, the model took less than 20 min where humans would need to manually (1) complete the 3D modeling (mean time 4.0 min), (2) run the 'Print' command on the 3D printer, and (3) remove the supporting material (mean time 5.6 min). As a result, the impact of labor costs may be small compared to the overall process. These results indicated that a 3D-printed model could be produced at a reasonable price and used on the same day once a CT was acquired. However, the cost-effectiveness of the model could not be easily assessed because the quality, size, and number of colors used in 3D printing differed depending on the study, and it was difficult to find a study that presented data on both cost and time. For two studies using high-quality and detailed 3D printing models, the cost amounted to hundreds of dollars, but the printing time was not reported [8,9]. Another study on lumbar spinal disease reported that its price per model was USD 30–45, but no printing time was provided [11]. In contrast, a study on articular fracture reported a printing time of 6–12 h, but the cost was not mentioned [31].

4.2.2. Usefulness of Personalized 3D-Printed Thyroid Gland Models

To evaluate the usefulness of the personalized 3D-printed thyroid models, two similar questionnaires were administered. The first questionnaire consisted of 12 items to compare two randomized groups of patients at the time of obtaining informed consent, while the second consisted of four items representing four categories and was provided to patients after surgery upon receiving their model.

For the first questionnaire, no significant differences existed between the two randomly assigned groups in terms of age, sex, diagnosis, pathological classification, and operation type (all $p > .05$). When the 12 items of the first questionnaire were grouped into four major categories (general knowledge,

benefits of surgery, risks of surgery, and satisfaction), the 3D-printed models significantly improved the scores in all categories (all $p < .05$). These results differed from those of a similar study on lung cancer, where only the knowledge category was rated significantly higher in the group that received 3D-printed models [9]. This conflicting result may be due to the smaller number of enrolled patients compared to this study. Another prospective study on thyroid cancer showed significant differences in anatomy, the relation of structures, and surgical procedures before and after providing an explanation using a common 3D phantom model [30]; however, it was not a randomized study and did not use personalized models.

In the second questionnaire, patients assigned the greatest value to "understanding the disease" (71.7%), followed by "overall satisfaction" (17.0%) and "understanding the operation" (11.3%). These results suggest that the mesh-type 3D modeling technique might have value for anatomical education, even though the models were not of high quality. The visualization of the location relationship between the tumor and thyroid gland may be the biggest advantage of this type of 3D-printed model.

4.2.3. Promising Utilization for Further Research

The deep learning algorithm for soft tissue segmentation trained on the thyroid gland can be used on other soft tissue lesions in the head and neck region, such as the oral cavity, lymph node, and salivary gland. In addition, without 3D printing, the obtained 3D modeling results can be displayed by using augmented reality or virtual reality technology. Further research should evaluate virtual visualization as a presurgical planning tool and surgical guide.

4.2.4. Limitation

There are several limitations to this study. Although the patients were randomly assigned to the two study groups, the clinician's explanations of consent for surgery could differ because the study was not double-blinded. In addition, the "understanding" of the patients was not evaluated objectively.

CT may not be a routine procedure for all thyroid surgeries. In the Republic of Korea, preoperative CT is covered by national insurance and is acceptable for the purposes of surgical planning, evaluation of regional metastasis, and preventing legal disputes; however, it may be unnecessary to perform CT scans for 3D printing in a different clinical setting.

Another important limitation is that incorporation of 3D-printed models

into patients' treatment could not be assessed, such as how it improved treatment outcomes or patients' care. It is necessary to expand the scope of application of the 3D model for each disease stage and treatment.

Finally, for the sake of reducing costs and time, the 3D-printed models were not of high quality. This limitation was mentioned in the discussion of the first experiment: thin-section CT scans (e.g., 1 mm splices) could provide more detailed information [41,42]; however, this could be harmful to patients by exposing them unnecessarily to additional radiation doses. From the results of the study, the specific purpose of educating a patient on thyroid surgery can be achieved even under conditions where only the minimum amount of necessary information is provided. Indeed, the approximate sizes of the thyroid glands and the locations of the tumors agreed well with those of the surgical specimens.

Chapter 5. Conclusions

The methodology of mesh-type 3D-modeling and personalized 3D-printed thyroid gland model fabrication was established in the experiments. In addition, the usefulness of personalized 3D-printed thyroid gland models in obtaining informed consent was confirmed. The 3D-printed model could improve a patient's understanding of the disease and surgery as well as their overall satisfaction. Although the quality of the mesh-type 3D-printed models was low, it was sufficiently effective to educate patients about the anatomy of the disease by illustrating the anatomical relationship between the tumor and thyroid gland and also improved overall patient satisfaction.

Personalized 3D models could be successfully created by using deep learning segmentation. Furthermore, the deep learning model was integrated successfully into a user-friendly application. The application allowed direct updating of the inferred result, thereby reducing the time required to prepare more training datasets to improve the performance of the deep learning model.

Finally, the newly devised mesh-type 3D modeling technique may facilitate the fabrication of anatomical models for personalized care, helping patients to conceptualize various organs, tumors, and surrounding tissues during informed surgical consent.

Acknowledgements

I am grateful to **Mr. Sungmin Yoon** (**SY**, Division of Convergence Technology, National Cancer Center) for printing and post-processing the 3D models and administering the randomization list; thank you to **Drs. Chang Hwan Ryu (CHR), Junsun Ryu (JR), and Yuh-Seog Jung (YSJ**) for handling patient enrollment and conducting the surgery.

This dissertation was reproduced with permission from "**Mesh-Type Three-Dimensional (3D) Printing of Human Organs and Tumors: Fast, Cost-Effective, and Personalized Anatomic Modeling of Patient-Oriented Visual Aids (Appl. Sci., 2021)**" and "**A Personalized 3D-Printed Model for Obtaining Informed Consent Process for Thyroid Surgery: A Randomized Clinical Study Using a Deep Learning Approach with Mesh-Type 3D Modeling (J. Pers. Med., 2021)**", copyrighted by MDPI.

Funding

This study was supported by a grant from the National Cancer Center, Republic of Korea [grant Nos. NCC2031580-1, NCC2010241-1, and NCC2020241-2].

Conflict of Interest and Financial Disclosure

Jungirl Seok (JS) is listed on a patent application describing similar methodology and filed by the National Cancer Center of Korea (Republic of Korea Patent No. 10-2227735, filed 3 January 2020, and issued 9 March 2021).

There are no financial ties to disclose.

Bibliography

1. Cho YB, Lee WY, Yun HR, Lee WS, Yun SH, Chun HK. Tumor localization for laparoscopic colorectal surgery. ***World J Surg***. 2007;31(7):1491-1495.
2. Hartl DM, Chami L, Al Ghuzlan A, Leboulleux S, Baudin E, Schlumberger M, Travagli JP. Charcoal suspension tattoo localization for differentiated thyroid cancer recurrence. ***Ann Surg Oncol***. 2009;16(9):2602-2608.
3. Yeung AR, Li JG, Shi W, Newlin HE, Chvetsov A, Liu C, Palta JR, Olivier K. Tumor localization using cone-beam CT reduces setup margins in conventionally fractionated radiotherapy for lung tumors. ***Int J Radiat Oncol Biol Phys***. 2009;74(4):1100-1107.
4. St. John M, Cowen MB, Smallman HS, Oonk HM. The use of 2D and 3D displays for shape-understanding versus relative-position tasks. ***Hum Factors***. 2001;43(1):79-98.
5. Wang Y, Zhao L, Wang M, Song Z. Organ at risk segmentation in head and neck CT images using a two-stage segmentation framework based on 3D U-Net. ***IEEE Access***. 2019;7:144591-144602.
6. Gsaxner C, Pepe A, Li J, Ibrahimpasic U, Wallner J, Schmalstieg D, Egger J. Augmented reality for head and neck carcinoma imaging: Description and feasibility of an instant calibration, markerless approach. ***Comput Methods Programs Biomed***. 2021;200:105854.
7. Rose AS, Kim H, Fuchs H, Frahm JM. Development of augmented-reality applications in otolaryngology–head and neck surgery**.** ***Laryngoscope***. 2019;129:S1-S11.
8. Tack P, Victor J, Gemmel P, Annemans L. 3D-printing techniques in a medical setting: a systematic literature review. ***Biomed Eng Online***. 2016;15(1):115.
9. Bernhard JC, Isotani S, Matsugasumi T, Duddalwar V, Hung AJ, Suer E, Baco E, Satkunasivam R, Djaladat H, Metcalfe C, Hu B, Wong K, Park D, Nguyen M, Hwang D, Bazargani ST, de Castro Abreu AL, Aron M, Ukimura O, Gill IS. Personalized 3D printed model of kidney and tumor anatomy: a useful tool for patient education. ***World J Urol***. 2016;34(3):337-345.
10. Yoon SH, Park S, Kang CH, Park IK, Goo JM, Kim YT. Personalized 3D-Printed Model for Informed Consent for Stage I Lung Cancer: A Randomized Pilot Trial. ***Semin Thorac Cardiovasc Surg***. 2019 Summer;31(2):316-318.
11. Zhuang YD, Zhou MC, Liu SC, Wu JF, Wang R, Chen CM. Effectiveness of personalized 3D printed models for patient education in degenerative lumbar disease. ***Patient Educ Couns***. 2019;102(10):1875-1881.
12. Yan Q, Dong H, Su J, Han J, Song B, Wei Q, Shi Y. A review of 3D printing technology for medical applications. ***Engineering***. 2018;4(5):729-742.
13. Mazur DJ. Consent and informed consent: their ongoing evolutions in clinical care and research on humans. ***Sociol Compass***. 2008;2(1):253-267.
14. Chan Y, Irish JC, Wood SJ, Rotstein LE, Brown DH, Gullane PJ, Lockwood

GA. Patient education and informed consent in head and neck surgery. ***Arch Otolaryngol Head Neck Surg***. 2002;128(11):1269-1274.
15. Lavelle-Jones C, Byrne DJ, Rice P, Cuschieri A. Factors affecting quality of informed consent. ***BMJ***. 1993;306(6882):885-890.
16. Hutson MM, Blaha JD. Patients' recall of preoperative instruction for informed consent for an operation. ***J Bone Joint Surg Am***. 1991;73(2):160-162.
17. Hekkenberg RJ, Irish JC, Rotstein LE, Brown DH, Gullane PJ. Informed consent in head and neck surgery: how much do patients actually remember? ***J Otolaryngol***. 1997;26(3):155-159.
18. Tait AR, Voepel-Lewis T. Digital multimedia: a new approach for informed consent? ***JAMA***. 2015;313(5):463-464.
19. Gabay G, Bokek-Cohen Y. Infringement of the right to surgical informed consent: negligent disclosure and its impact on patient trust in surgeons at public general hospitals–the voice of the patient. ***BMC Med Ethics***. 2019;20(1):1-13.
20. Nehme J, El-Khani U, Chow A, Hakky S, Ahmed AR, Purkayastha S. The use of multimedia consent programs for surgical procedures: a systematic review. ***Surg Innov***. 2013;20(1):13-23.
21. Rosenfeld EH, Lopez ME, Yangyang RY, Justus CA, Borges MM, Mathai RC, Karediya A, Zhang W, Brandt ML. Use of standardized visual aids improves informed consent for appendectomy in children: A randomized control trial. ***Am J Surg***. 2018;216(4):730-735.
22. Moseley TH, Wiggins MN, O'Sullivan P. Effects of presentation method on the understanding of informed consent. ***Br J Ophthalmol***. 2006;90(8):990-993.
23. O'Brien EK, Wayne DB, Barsness KA, McGaghie WC, Barsuk JH. Use of 3D printing for medical education models in transplantation medicine: a critical review. ***Curr Transplant Rep***. 2016;3(1):109-119.
24. Kurenov SN, Ionita C, Sammons D, Demmy TL. Three-dimensional printing to facilitate anatomic study, device development, simulation, and planning in thoracic surgery. ***J Thorac Cardiovasc Surg***. 2015;149(4):973-979 e971.
25. Chan HH, Siewerdsen JH, Vescan A, Daly MJ, Prisman E, Irish JC. 3D Rapid Prototyping for Otolaryngology-Head and Neck Surgery: Applications in Image-Guidance, Surgical Simulation and Patient-Specific Modeling. ***PLoS One***. 2015;10(9):e0136370.
26. Craft DF, Howell RM. Preparation and fabrication of a full-scale, sagittal-sliced, 3D-printed, patient-specific radiotherapy phantom. ***J Appl Clin Med Phys***. 2017;18(5):285-292.
27. Hong D, Lee S, Kim T, Baek JH, Lee Y-m, Chung K-W, Sung T-Y, Kim N. Development of a personalized and realistic educational thyroid cancer phantom based on CT images: An evaluation of accuracy between three different 3D printers. ***Comput Biol Med***. 2019;113:103393.

28. Hazelaar C, van Eijnatten M, Dahele M, Wolff J, Forouzanfar T, Slotman B, Verbakel WF. Using 3D printing techniques to create an anthropomorphic thorax phantom for medical imaging purposes. ***Med Phys***. 2018;45(1):92-100.
29. Osti F, Santi GM, Neri M, Liverani A, Frizziero L, Stilli S, Maredi E, Zarantonello P, Gallone G, Stallone S. CT conversion workflow for intraoperative usage of bony models: From DICOM data to 3D printed models. ***Appl Sci***. 2019;9(4):708.
30. Hong D, Lee S, Kim T, Baek JH, Kim WW, Chung KW, Kim N, Sung TY. Usefulness of a 3D-Printed Thyroid Cancer Phantom for Clinician to Patient Communication. ***World J Surg***. 2020;44(3):788-794.
31. Bizzotto N, Tami I, Santucci A, Romani D, Cosentino A. 3D Printed replica of articular fractures for surgical planning and patient consent: A 3 years multi-centric experience. ***Mater Today Commun***. 2018;15:309-313.
32. Mason D. SU-E-T-33: pydicom: an open source DICOM library. ***Med Phys***. 2011;38(6Part10):3493-3493.
33. Vollmer J, Mencl R, Mueller H. in Computer graphics forum. 131-138 (Wiley Online Library).
34. Ronneberger O, Fischer P, Brox T. in International Conference on Medical image computing and computer-assisted intervention. 234-241 (Springer).
35. Champely S, Ekstrom C, Dalgaard P, Gill J, Weibelzahl S, Anandkumar A, Ford C, Volcic R, De Rosario H, De Rosario MH. Package 'pwr'. R package version. 2018;1(2).
36. Lidz CW. The therapeutic misconception and our models of competency and informed consent. ***Behav Sci Law***. 2006;24(4):535-546.
37. Garcia J, Yang Z, Mongrain R, Leask RL, Lachapelle K. 3D printing materials and their use in medical education: a review of current technology and trends for the future. ***BMJ Simul Technol Enhanc Learn***. 2018;4(1).
38. Haugen BR, Alexander EK, Bible KC, Doherty GM, Mandel SJ, Nikiforov YE, Pacini F, Randolph GW, Sawka AM, Schlumberger M, Schuff KG, Sherman SI, Sosa JA, Steward DL, Tuttle RM, Wartofsky L. 2015 American Thyroid Association Management Guidelines for Adult Patients with Thyroid Nodules and Differentiated Thyroid Cancer: The American Thyroid Association Guidelines Task Force on Thyroid Nodules and Differentiated Thyroid Cancer. ***Thyroid***. 2016;26(1):1-133.
39. Masumoto J, Hori M, Sato Y, Murakami T, Johkoh T, Nakamura H, Tamura S. Automated liver segmentation using multislice CT images. ***Syst Comput Japan***. 2003;34(9):71-82.
40. Shiffman S, Rubin GD, Napel S. Medical image segmentation using analysis of isolable-contour maps. ***IEEE Trans Med Imaging***. 2000;19(11):1064-1074.
41. Zhang Y, Zhou Y, Yang X, Tang P, Qiu Q, Liang Y, Jiang J. Thin slice three dimentional (3D) reconstruction versus CT 3D reconstruction of human breast cancer. ***Indian J Med Res.*** 2013;137(1):57-62.

42. Kim JS, Kim JH, Cho G, Bae KT. Automated detection of pulmonary nodules on CT images: effect of section thickness and reconstruction interval—initial results. ***Radiology***. 2005;236(1):295-299.

Abstract in Korean

국문 초록

종양의 3차원적 위치 파악을 위한 메쉬 구조의 3D 모델링 기술 개발 및 임상적 유용성 평가

서울대학교 대학원
의학과 의공학 전공
석 준 걸

배 경: 3D 프린팅은 인체 종양의 3차원적 위치를 파악하기 위한 방법으로써, 이미 의학 영역에 다양한 목적으로 보급되어 사용되고 있으나, 높은 비용과 긴 제작 시간은 3D 모델의 활용에 제약이 되고 있다.

목 적: 첫 번째 연구의 목표는 인체 장기와 그 장기가 포함하고 있는 종양의 관계를 묘사하기 위해 메쉬 구조의 3D 모델링이라고 하는 새로운 기법을 개발하는 것으로, 비용의 절감 및 출력 시간에서 장점을 보일 것으로 가정하였다. 두 번째 연구는 딥러닝을 이용한 개별화된 3D 갑상선 모델을 메쉬 구조로 제작하고 수술 전 동의를 받는 과정에 이용하여 본 기술의 임상적 유용성을 평가하고자 하였다.

방 법: 메쉬 구조의 3차원 모델링은 단층 영상에서 일정 간격으로 좌표를 추출하고, 이를 그물망(메쉬) 형태로 연결하는 구조의 레플리카를 생성한다. 인접한 해부학적 구조는 메쉬의 밀도를 변화시켜 출력하는 방식으로 구분할 수 있으며, 정상 조직과 종양은 대조되는 색상으로 표시한다. 이를 이용한 임상 연구를 위해, 수술 전 동의서 작성에 3D 모형을 이용하는 전향적 무작위 배정 대조군 비교 임상시험(KCT0005069)을 설계하였다. 갑상선 수술을 받는 환자 53명을 대상으로, 수술 동의서 작성 시 개별화된 3D 프린팅 모델을 사용하는 군과, 사용하지 않고 기존

의 방식대로 동의서를 작성하는 두 그룹으로 나누었다. 이 과정에서 U-Net 기반의 딥러닝 아키텍처와 메쉬 구조의 3D 모델링 기법을 활용하여 개인화된 3D 모델을 제작하였다.

결 과: 메쉬 구조의 3D 모델링을 이용해 융합 적층 모델링(FDM) 방식의 3D 프린터를 통해 출력한 결과, 낮은 비용($0.05/$cm^3$)과 제작 시간(1.73 min/$cm^3$)을 보였다. 실제 3D 프린팅 된 모형은 수술 중 절제된 검체와 비교했을 때 장기-종양 해부학 및 인접 조직을 시각적으로 구분하는데 충분한 수준을 보였다. 이후 시행한 전향적 임상 연구에서, 53명의 환자들의 갑상선 모형의 평균 3D 프린팅 시간은 258.9분이었고 평균 제작비는 환자 1인당 USD 4.23였다. 모든 3차원 모형은 종양과 갑상선의 크기, 위치, 해부학적 관계를 효과적으로 반영할 수 있었다. 수술 동의서 작성시 개별화된 3D 프린팅 모델을 제공받은 그룹은 4가지 범주(일반 지식, 수술의 이점, 수술의 위험, 만족도) 모두에서 통계적으로 유의한 수준의 개선을 보였다 (모두 p <0.05). 모든 환자는 수술 후 개별화된 3D 모델을 제공받았으며, 질병, 수술 및 가능한 합병증 및 전반적인 만족도 향상에 도움이 되었음을 확인할 수 있었다.

결 론: 개별화된 3D 갑상선 모델은 수술 전 동의서 작성 과정에서 환자의 이해와 만족도를 향상시키는 효과적인 도구가 될 수 있었다. 새롭게 고안한 메쉬 구조의 3D 모델링 기법은 장기의 크기/윤곽 및 종양의 위치를 시각화 하는데 효과적이었으며, 이러한 방법론은 개별화된 치료를 위한 해부학적 모델링을 용이하게 하고, 수술 동의서 작성과 같은 설명 과정에 있어, 환자의 효과적인 의학적 지식 습득을 도울 수 있음을 확인하였다.

주요어: 메쉬 구조의 3D 모델링; 3D 프린팅; 수술 동의서 작성; 갑상선; 적층형 출력; 딥러닝

학 번: 2014-21979